Patterning Polymers at the Nanoscale

Dr Joachim H. G. Steinke

Department of Chemistry
Imperial College London
j.steinke@imperial.ac.uk

Lecture Content

- Patterning with "Light"
  - Photolithography
  - Optical Interference Patterns

- Physical Contact Patterning
  - Soft Lithography
  - Surface Imprinting (Embossing)

- Self-Assembly
  - Copolymer Self-Assembly
  - Molecularly Imprinted Polymers

- Direct Write
  - Dip-Pen Nanolithography
  - Inkjet Printing

Strategies – Intrinsic Limitations

pattern formation using[a]	basis for intrinsic limitations	strategies to circumvent the limitations
photons		
UV, DUV, EUV, and X-rays	diffraction	contact mode, near-field exposure
	depth of focus	nonlinear photoresists
particles		
electrons and ions	electrostatic interactions	neutral atoms
	writing is serial	projection
	small field of writing	arrays of sources
neutral atoms	de Broglie wavelength	
machining		
AFM, STM, NSOM, and electrochemical	writing is serial	arrays of probes
	small field of writing	
physical contact	van der Waals forces	
printing, molding, and embossing	speed of capillary filling	low-viscosity solutions
	adhesion of mold and replica	surface modification
self-assembly	control over order, domain size, and density of defects	
surfactant systems		
block copolymers		
crystallization of proteins and colloids		
deposition	low flexibility in patterning and fabrication of masks or templates	
cleaved edge overgrowth		
shadowed evaporation		
size reduction		
glass drawing	low flexibility in patterning; reproducibility	
compression of elastomeric masters or molds		
controlled reactive spreading		
edge-based technologies		
near-field phase-shifting photolithography	diffraction	
topographically directed photolithography	diffraction	
topographically directed etching		

[a] Abbreviations: UV (ultraviolet), DUV (deep ultraviolet), EUV (extreme ultraviolet); AFM (atomic force microscope); STM (scanning tunneling microscope); and NSOM (near-field scanning optical microscope).

New Technologies - Flexible

pattern formation using	writing	replication	refs
physical contact			
nanomachining (STM, AFM, NSOM, and electrochemical methods)	yes	no	144−159
soft lithography (μCP, MIMIC, μTM, REM, and SAMIM)	no	yes	38, 161
embossing/imprinting	no	yes	88, 91, 194
photons			
near-field phase-shifting photolithography	no[b]	yes	39, 201, 203
topographically directed photolithography	no[b]	yes	204
deposition			
topographically directed etching	no[b]	yes	205
particles			
metastable atom lithography	no	yes	209, 210
size reduction			
glass drawing	yes	no	122−124
compression of elastomeric mold	yes	yes	125−127
shadowed evaporation	yes	no	114−116
controlled reactive spreading	yes	no	191

[a] In this table, yes means this technique is practical for writing or replication of features of ≤100 nm; no means this technique cannot practically be so used. [b] With possible specialized exceptions.

Regular or Simple Nanopatterns

pattern formation using	writing	replication	refs
photons			
holographic lithography	yes	yes	214−221
deposition			
laser-focused deposition	yes	no	165, 223, 224
cleaved edge overgrowth	yes	no	113, 259, 260
self-assembly			
crystallization of proteins, colloids, and microspheres	yes	no	226−242
microphase separation of block copolymers	yes	no	106, 246−251
other			
anodic oxidation of aluminum	yes	no	252−257

[a] In this table, yes means this technique is practical for writing or replication of features of ≤100 nm; no means this technique cannot practically be so used.

Patterning with "Light"

Photolithography – Composite Resists

(A) Scheme representing the preparation of masters with features down to 100 nm using phase-shifting photolithography.

(B) Illustration depicting the types of nanostructures generated in positive- and negative-tone resist through phase-shifting masks molded against masters from (A).
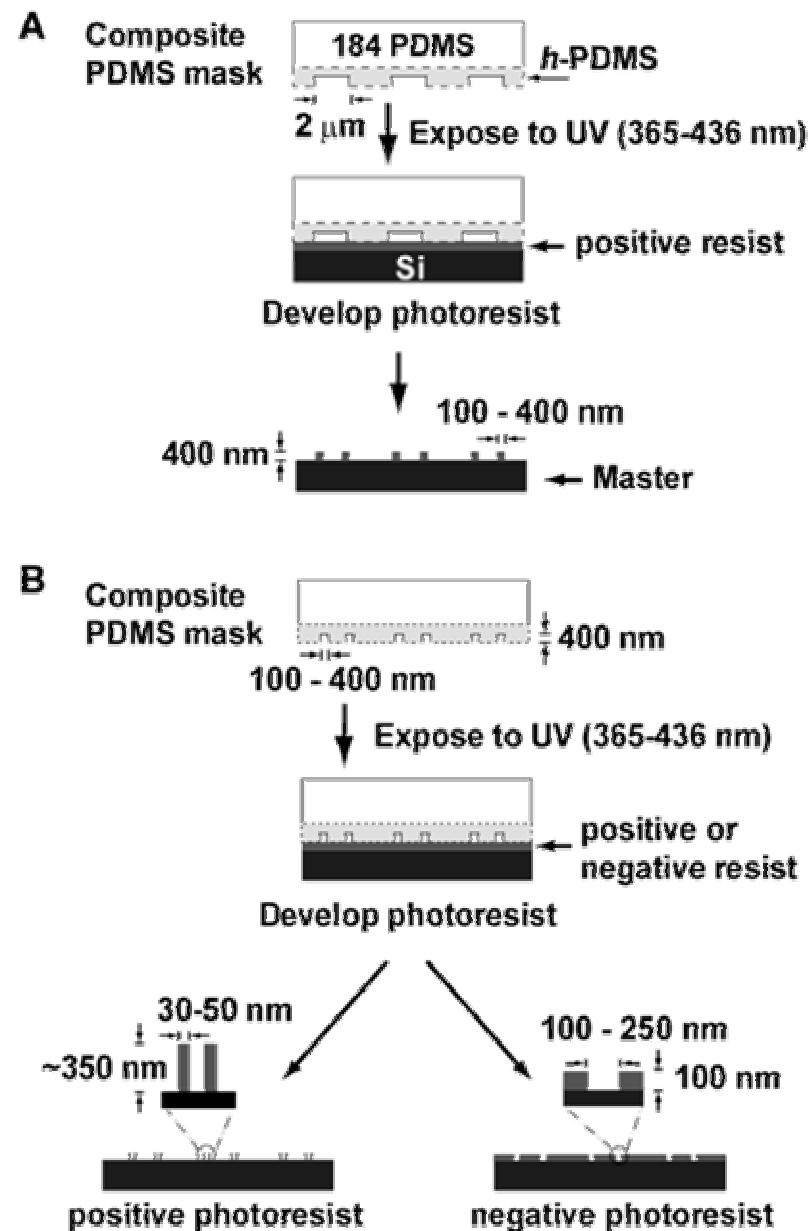
Photolithography – Composite Resists

(A and B) Scanning electron micrographs (SEM) of rings of photoresist. Light regions are photoresist, and dark regions are Si/SiO$_2$. (C and D) Arrays of rings etched in palladium films (bright) supported on Si substrates (dark) generated from masters having 250 nm diameter and 350 nm diameter posts. (E) Array of individual NaCl crystals crystallized in 250 nm diameter wells. (F) Array of 30 nm NaCl nanocrystals in 100 nm diameter wells.
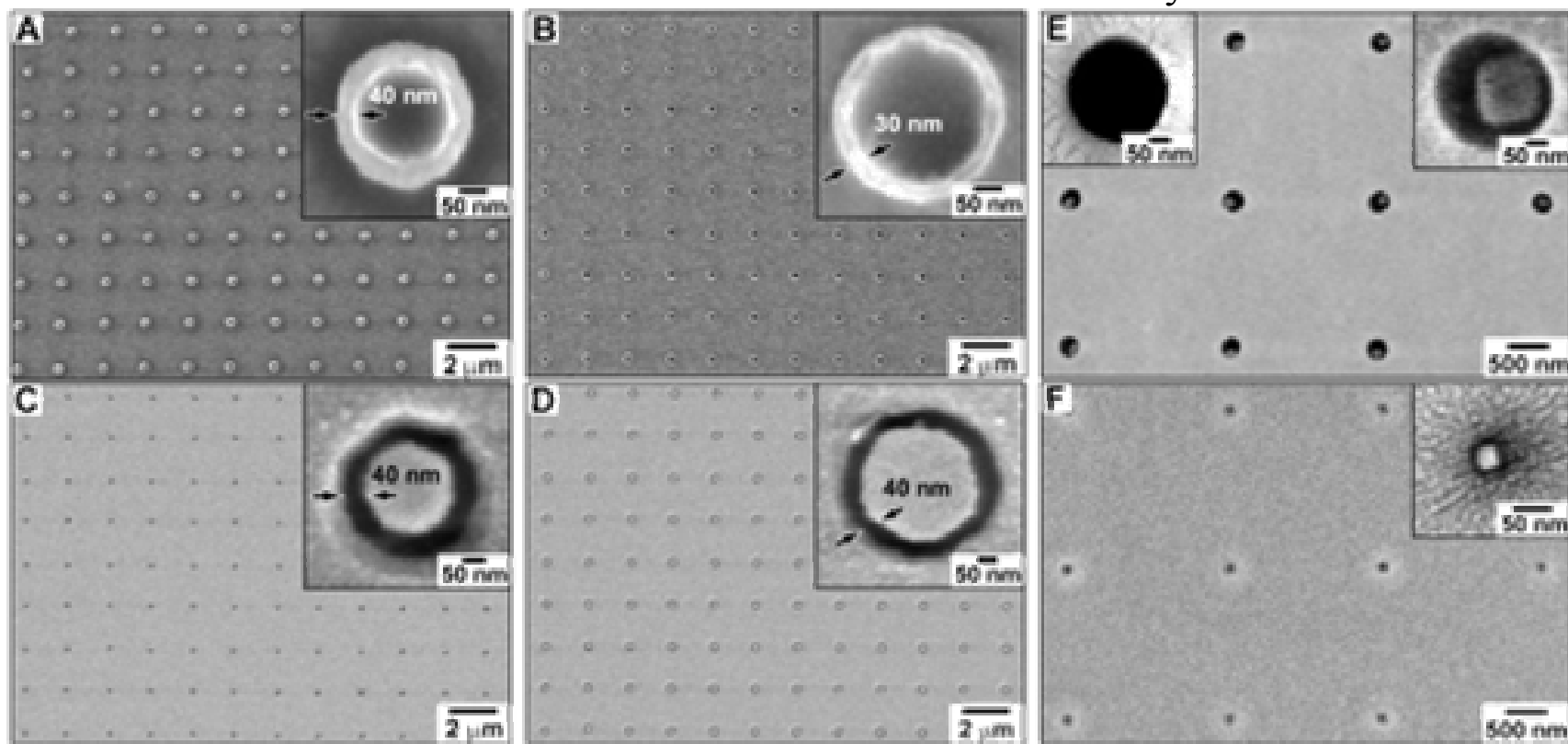
E- Beam Photoresist Composites

SEM images of patterns (writing beam size: 60 nm) delineated on 280 nm-thick films (a and b) of 4 wt.% SiO_2 incorporated ZEP520®

and (c and d). on ZEP520®

The parameters are 150 C/cm^2 at 50 keV (a and c) and 210 C/cm^2 at 100 keV (b and d).
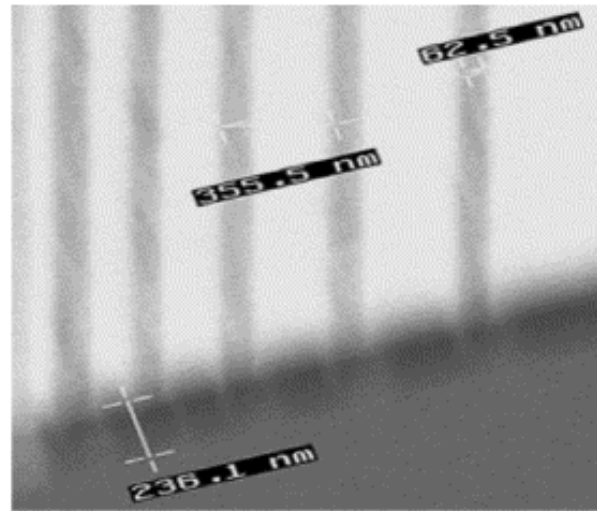
(a)
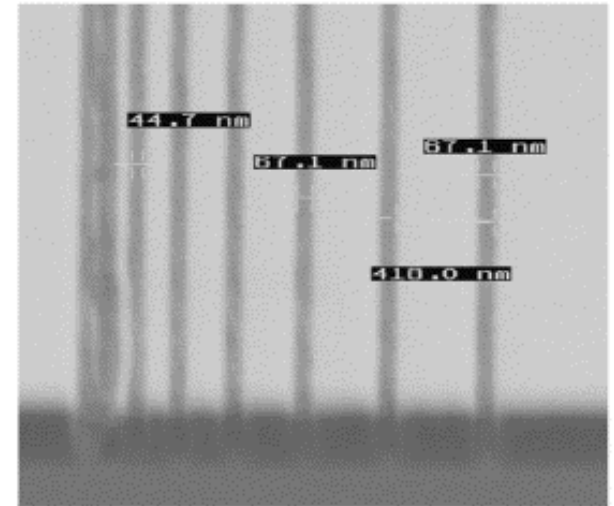
(b)
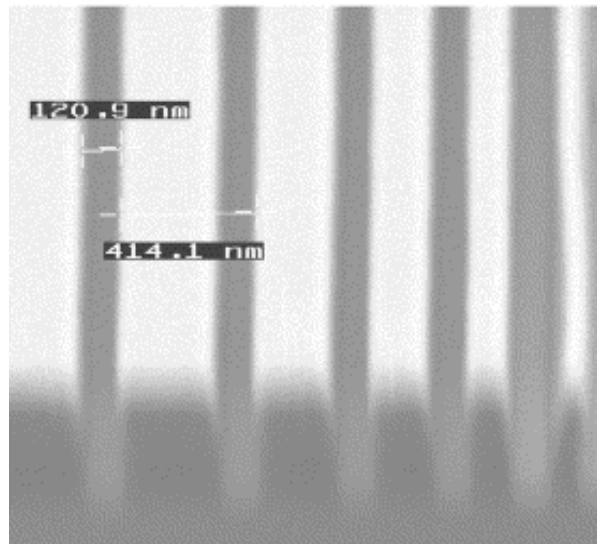
(c)
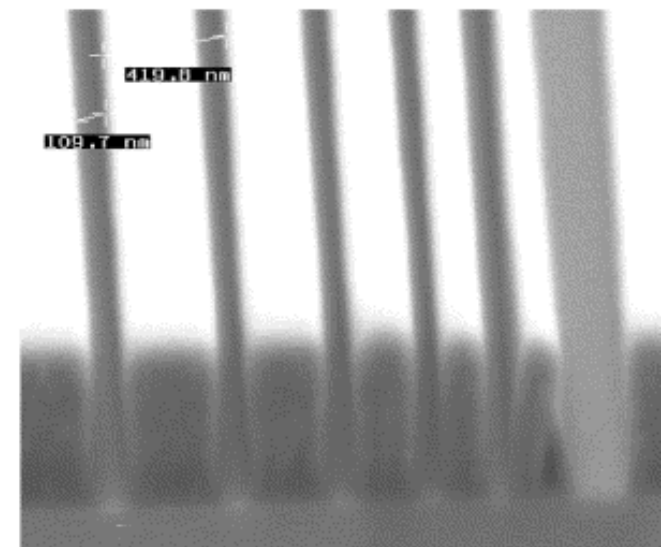
(d)

E-Beam Composite Photoresists
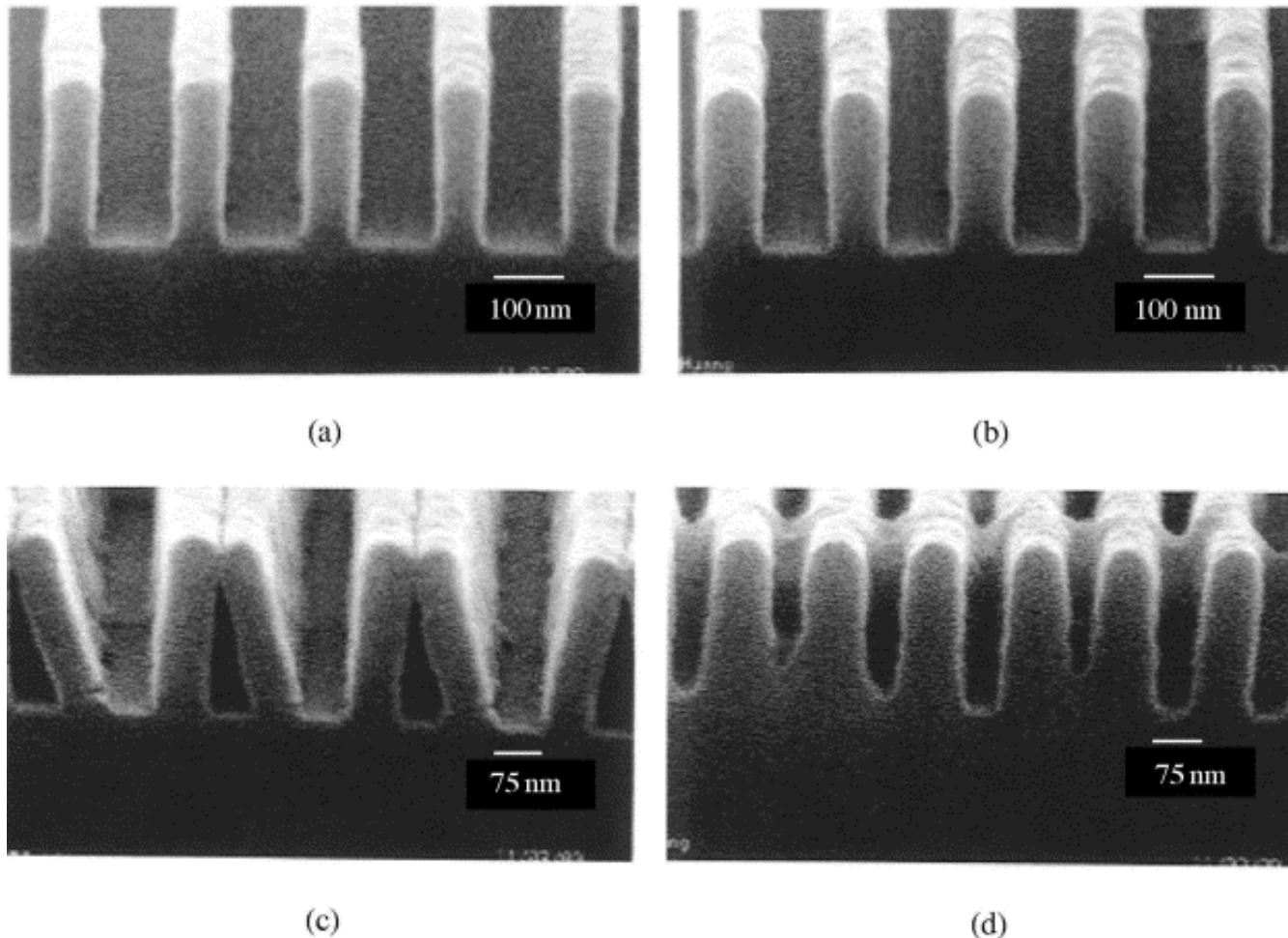
Comparison between patterns obtained after writing 100- and 75-nm l/s on the KRS-XE® film (a and c, respectively) and on its silica/KRS-XE nanocomposite counterpart (band d, respectively) at a dose of 26 C/cm^2 with a 75-keV e-beam.

LB Film Photoresists

Schematic illustration of the p(DDA-*t*BVPC) monolayer on the water surface.
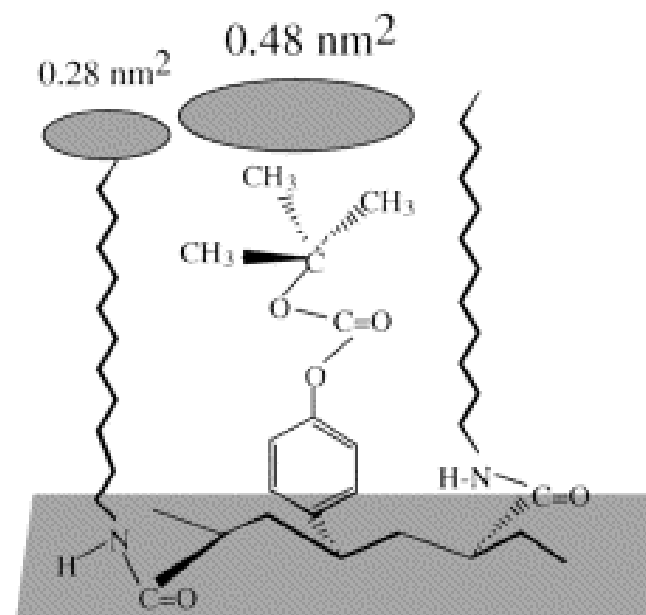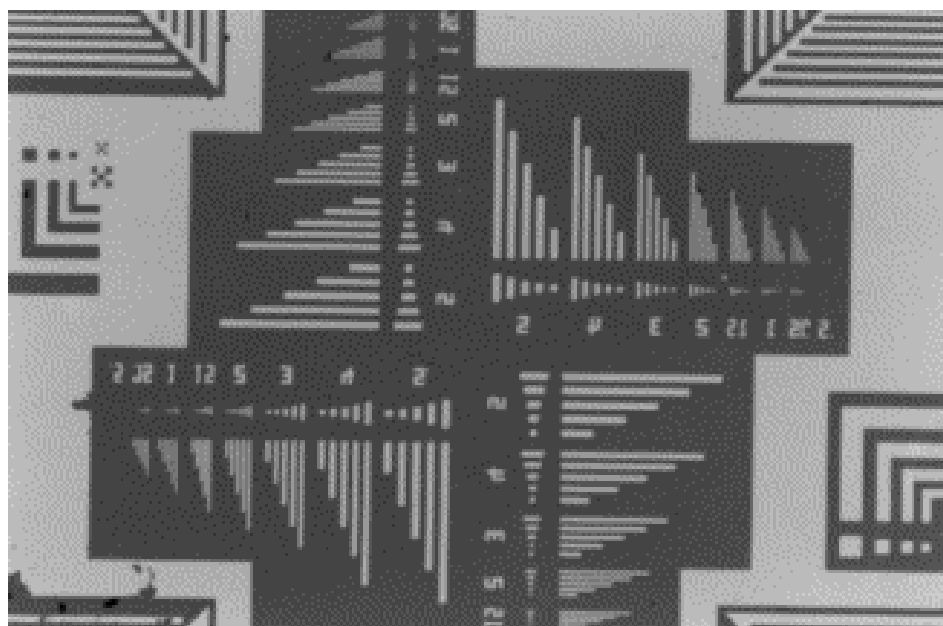
Optical micrograph of positive fine patterns with p(DDA-*t*BVPC53) LB films (40 layers) on a silicone wafer after UV irradiation following development with 10% TMAH aqueous solution.

Near Field Azo PMMA – Data Storage

a) 5µm×5µm shear force image of the pattern on the PMA4 film obtained illuminating the sample for 1 s at 325 nm.

(b) Profile analysis along the black line marked in the image.
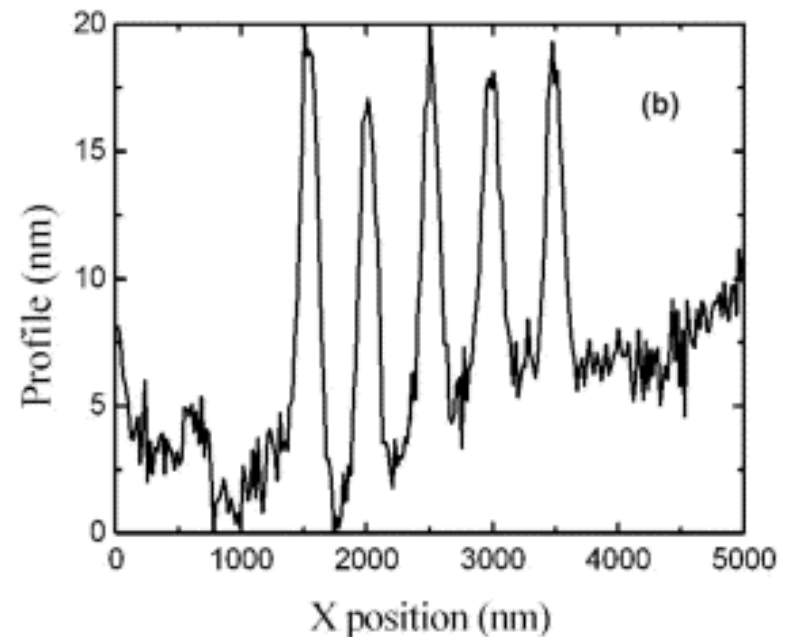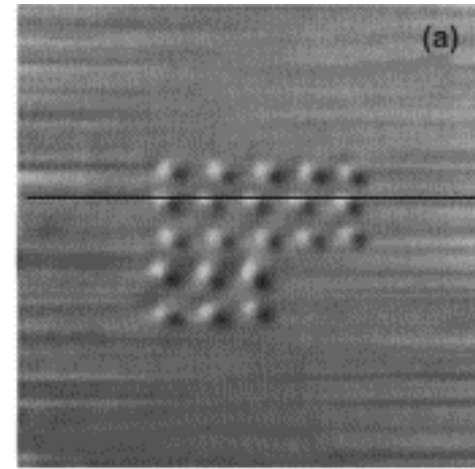
Near Filed Azo PMMA

Three dots obtained with different exposure times upon Ar$^+$ laser illumination at 488 nm. The embossing grows linearly with the exposure time.
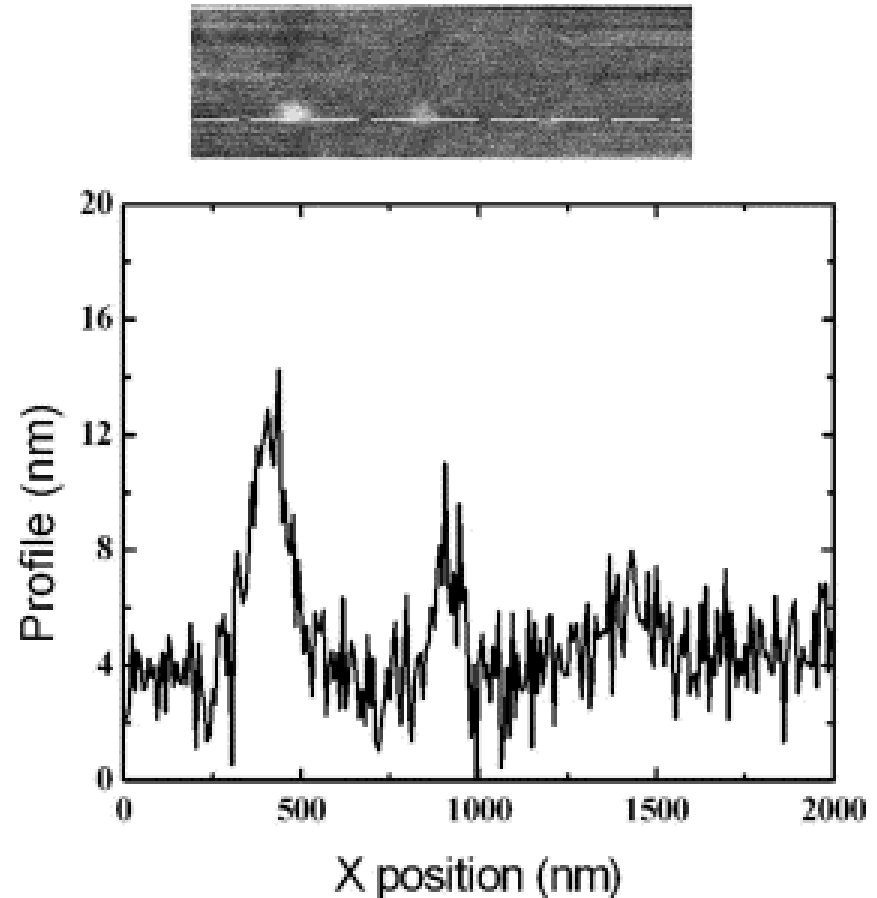
Two-Photon Generated Photoacid
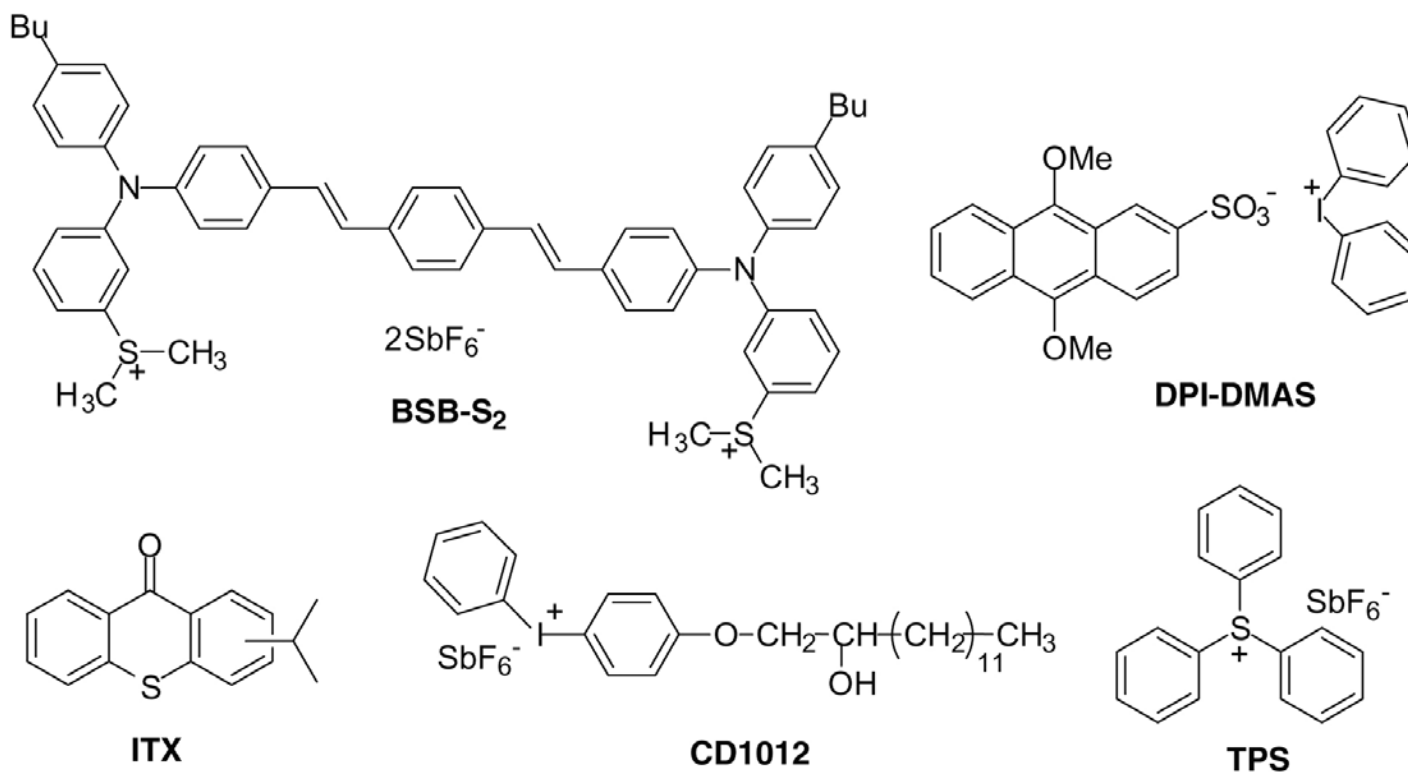
Structures of BSB-S$_2$ and the commercially available PAGs used in this study: DPI-DMAS, diphenyliodonium 9,10-dimethoxyanthracenesulfonate; ITX, isopropylthioxanthone; CD1012, [4-[(2-hydroxytetradecyl)oxy]phenyl]phenyliodonium hexafluoroantimonate (Sartomer); and TPS, triphenylsulfonium hexafluoroantimonate

Two-Photon Generated Photoacid

A 3D microchannel structure fabricated by two-photon exposure of BSB-S$_2$ in THPMA-MMA. After irradiation, the film was baked for 1 min at 90°C. The target structure was then obtained by dissolving the exposed resin in aqueous 0.26 M tetramethyl ammonium hydroxide.

(**A**) rectangular cavities (width, 100 μm; length, 20 μm; depth, 20 μm) with a sloped side wall that are connected by 12 channels (**B**) SEM of the final structure

Two-photon fluorescence images of the final structure (**C**) at the surface of the film, (**D**) 10 μm below the surface, and (**E**) 19 μm below the surface. (**F**) Buried channels.
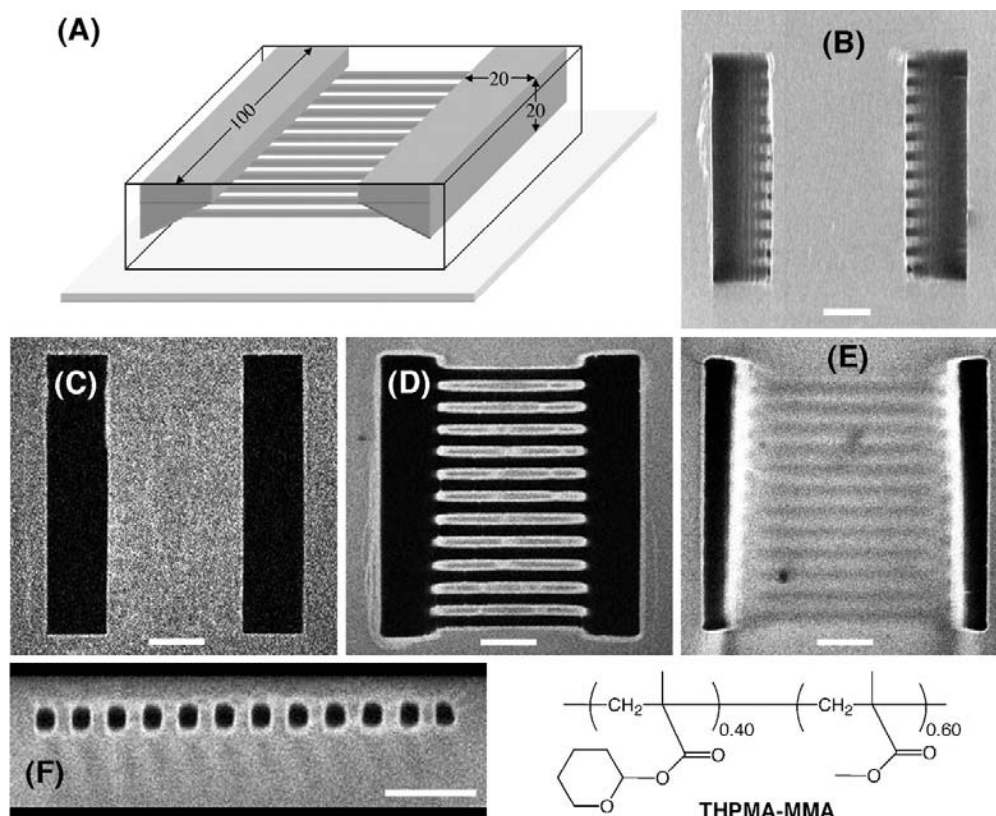
Two-Photon Photopolymerisation
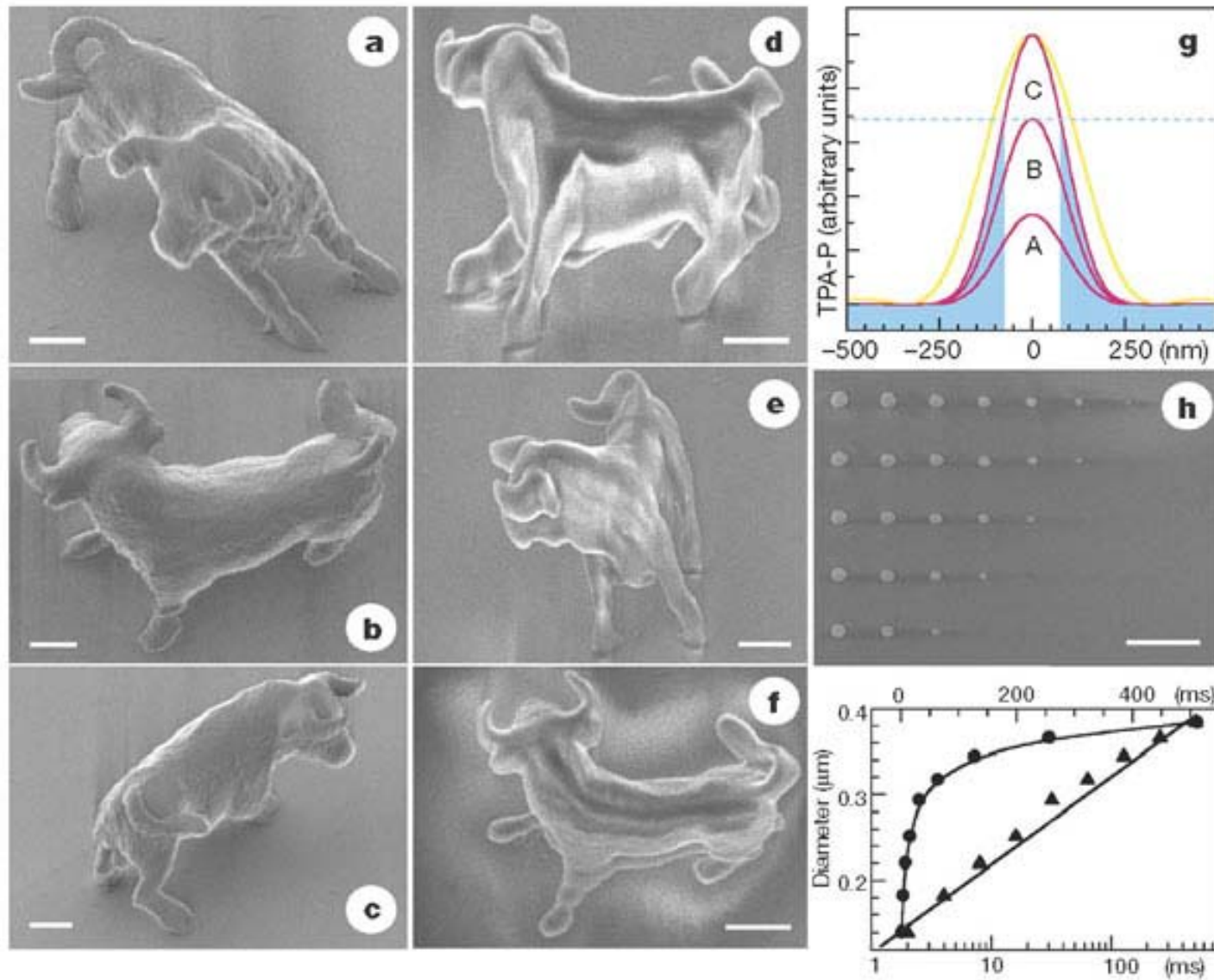
Two-Photon Polymerisation

Microfabrication and nanofabrication at subdiffraction-limit resolution. **a–c,** Bull sculpture produced by raster scanning; the process took 180 min. **d–f,** The surface of the bull was defined by two-photon absorption (TPA; that is, surface-profile scanning) and was then solidified internally by illumination under a mercury lamp. **g,** Achievement of subdiffraction-limit resolution, where A, B and C respectively denote the laser-pulse energy below, at and above the TPA-polymerization threshold (dashed line). The yellow line represents the range of single-photon absorption. TPA-P, TPA probability. **h,** Scanning electron micrograph of voxels formed at different exposure times and laser-pulse energies. **i,** Dependence of lateral spatial resolution on exposure time. The laser-pulse energy was 137 pJ. The same data are presented using both logarithmic (triangles; bottom axis) and linear (circles; top axis) coordinates, to show the logarithmic dependence and threshold behaviour of TPA photopolymerization. Scale bars, 2 μm.

Laser Tweezers

Geometry and picture of an efficient microscopic light driven rotor

(a) Explanatory drawing and

(b) photograph of the rotor in an arbitrary position when it is tumbling freely, viewed from identical directions.

(c) Drawing and

(d) equivalent photograph of the rotor when it is trapped in focus but held against the cover glass thereby preventing rotation and yielding a sharp image.

(e) Photograph of the spinning rotor trapped in focus and rotated by the light

3 μm
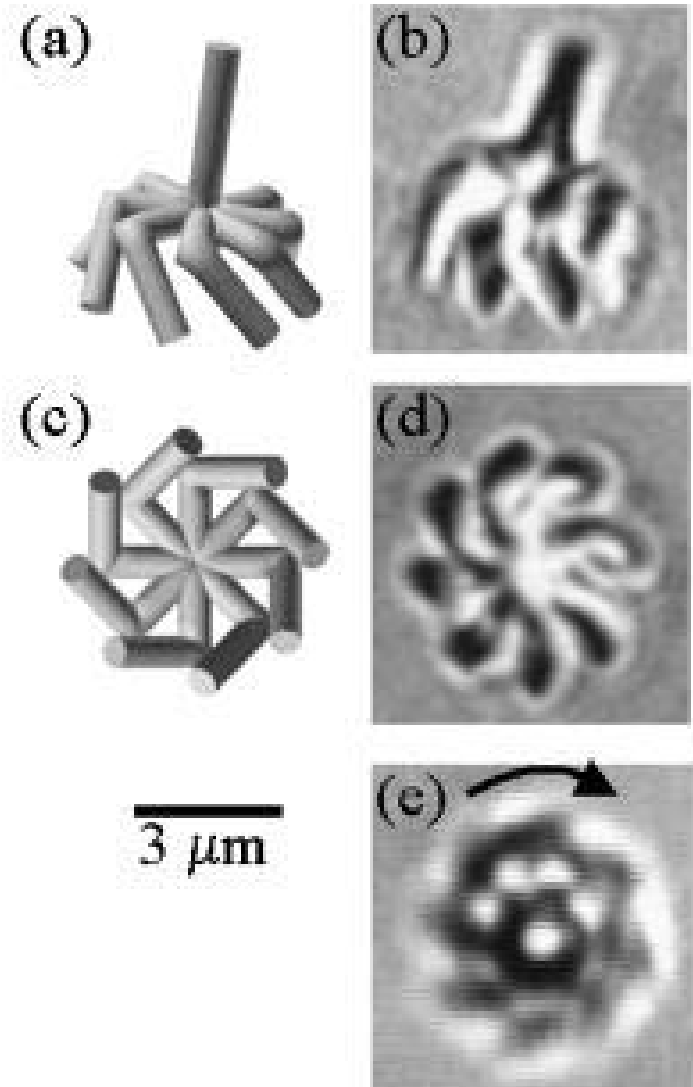
Laser Tweezers
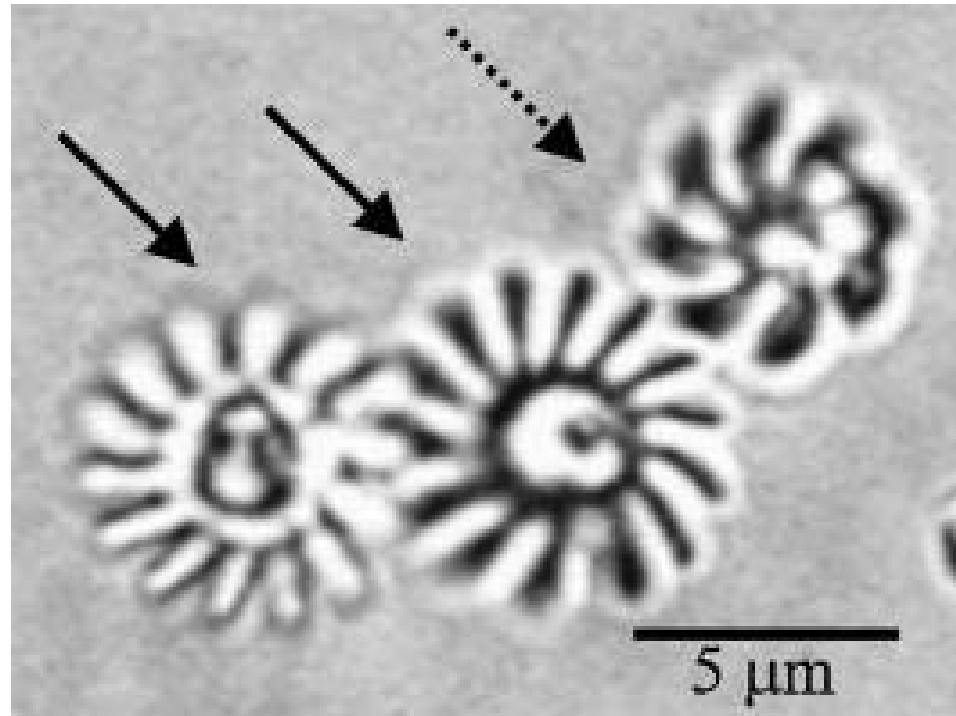
Complex micromachine built by the two-photon technique: two engaged cogwheels are rotated by a light driven rotor. The solid arrows point to the cogwheels rotating on axes fixed to the glass surface. The dashed arrow points to the rotor. The rotor is held and rotated by the laser tweezers and the rotating propeller drives the system.

Two-Photon Photopolymerisation

Functional micro-oscillator system, in which not only the spring but also the cubic anchor and the bead were produced using our two-photon absorption system. The oscillator was kept in ethanol so that the buoyancy would balance gravity and eliminate bead–substrate friction. **a, b,** The spring in its original (**a**) and extended (**b**) states. Scale bars, 2 μm. **c,** Restoring curve of the damping oscillation; inset, diagram showing driving of the oscillator by using laser trapping.
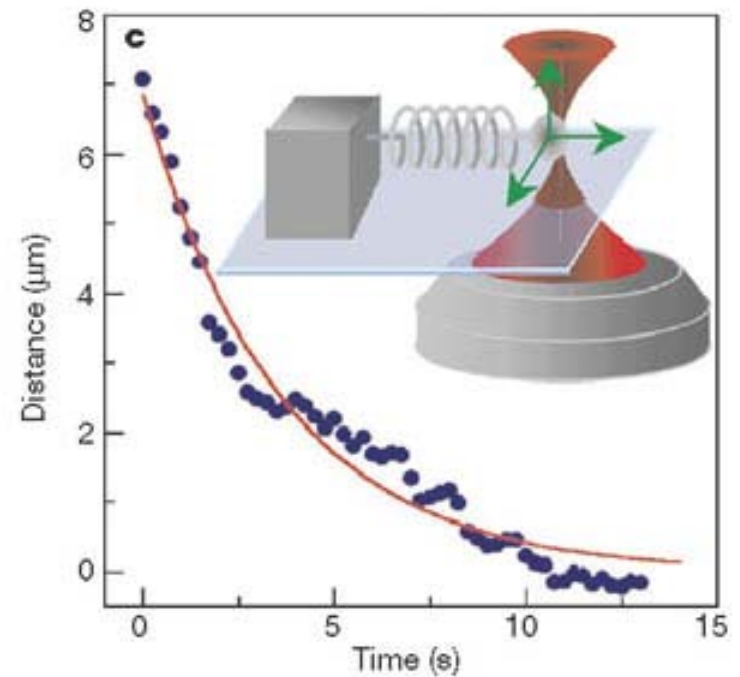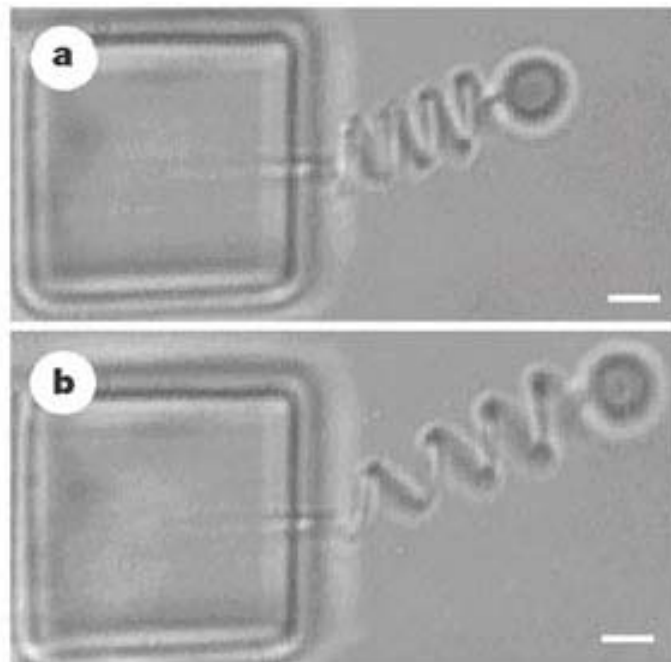
Physical Contact Patterning

Nanoimprint Lithography

SEM image of a print in a 1 μm thick PBAS (poly(phenyl-bis-4-amino-styrene)) film with a 200-nm deep silicon stamp. The polymer was cross-linked with a 17-s UV exposure. OBDUCAT NanoImprint NIL-2-OB-l unit, 30 bar,185 °C during 1 min.
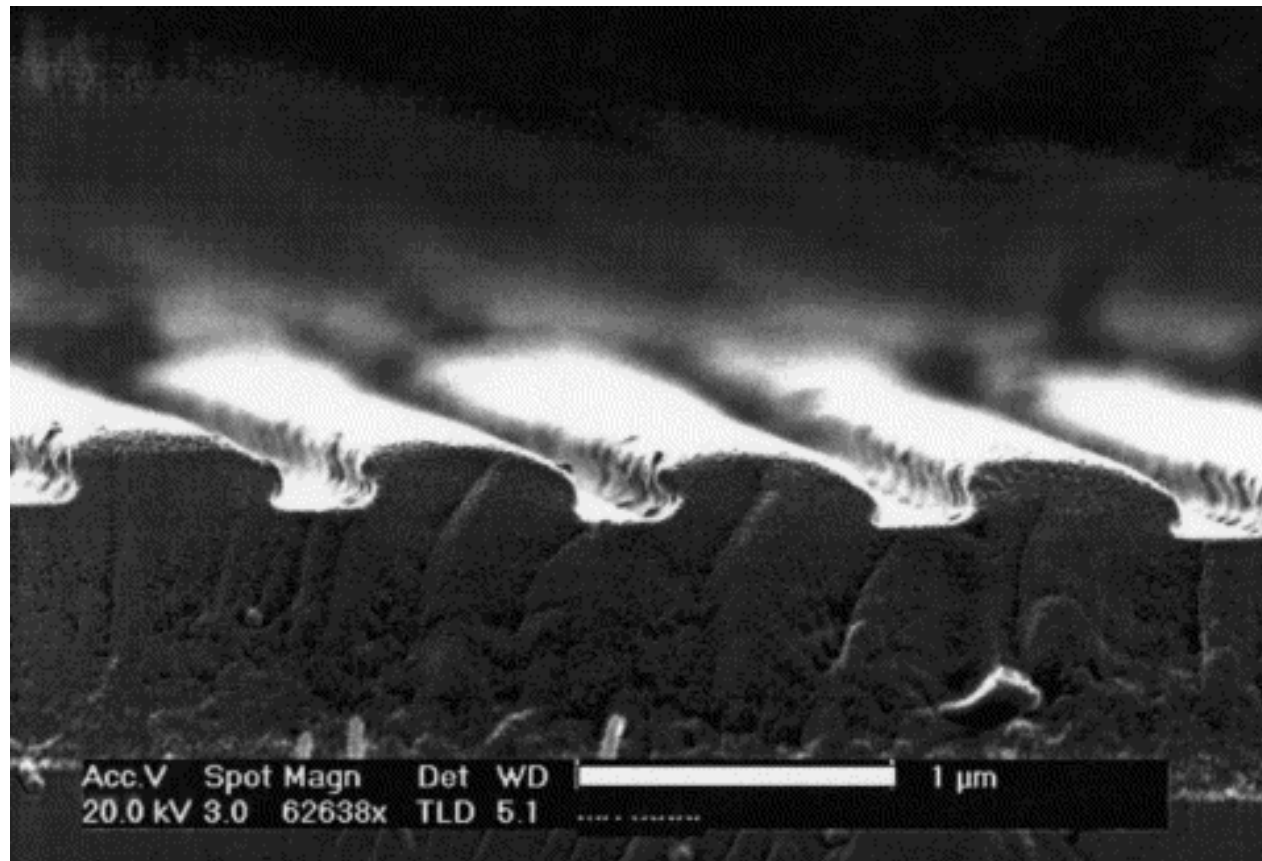
Soft Lithography

Schematic procedures describing soft lithographic methods [38,161] and near-field phase-shifting photo-lithography.[38,162]
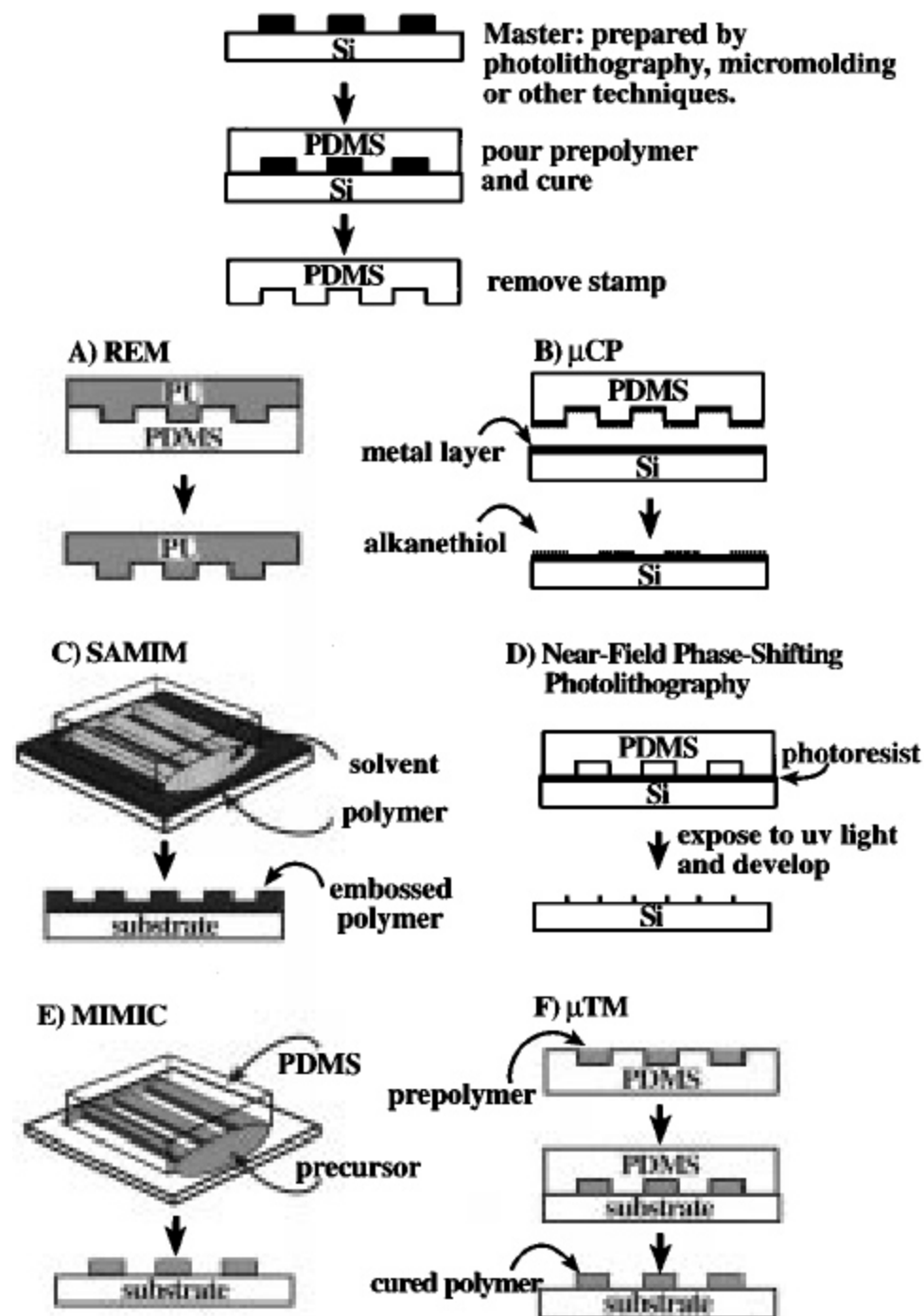
Nanopatterned LEDs

Steps for fabricating micropatterned polymer LEDs using solvent-assisted micromolding. Casting and curing a prepolymer of polydimethylsiloxane against a relief structure generates an elastomeric mold.

Wetting the surface of this mold with methanol and then bringing it into contact with a film of a PPV precursor spin cast onto an ITO/glass substrate softens the precursor and causes it to wick into the recessed regions of the mold. Removing the mold after the methanol evaporates leaves a film of precursor with surface relief that matches the mold; thermal conversion of the precursor yields PPV with the same surface relief.

The relief is preserved in this conversion because the change in volume is relatively small and because it occurs at temperatures less than the glass transition of the PPV or the partially converted precursor. Deposition of a bilayer cathode of Al (~ 200 nm) and Ca (~ 40 nm) onto the patterned PPV forms an electrically continuous layer and completes the fabrication.

Optical Micrographs of Emission	AFM Images of Surface Relief	Transmission Mode Optical Micrograph	Optical Micrograph of Emission

—5 μm

I 300 nm —5 μm

—5 μm

I 300 nm —5 μm

—10 μm

—5 μm

transmitted intensity — position

emitted intensity — position

transmitted intensity — ~800 nm — position

emitted intensity — ~800 nm — position
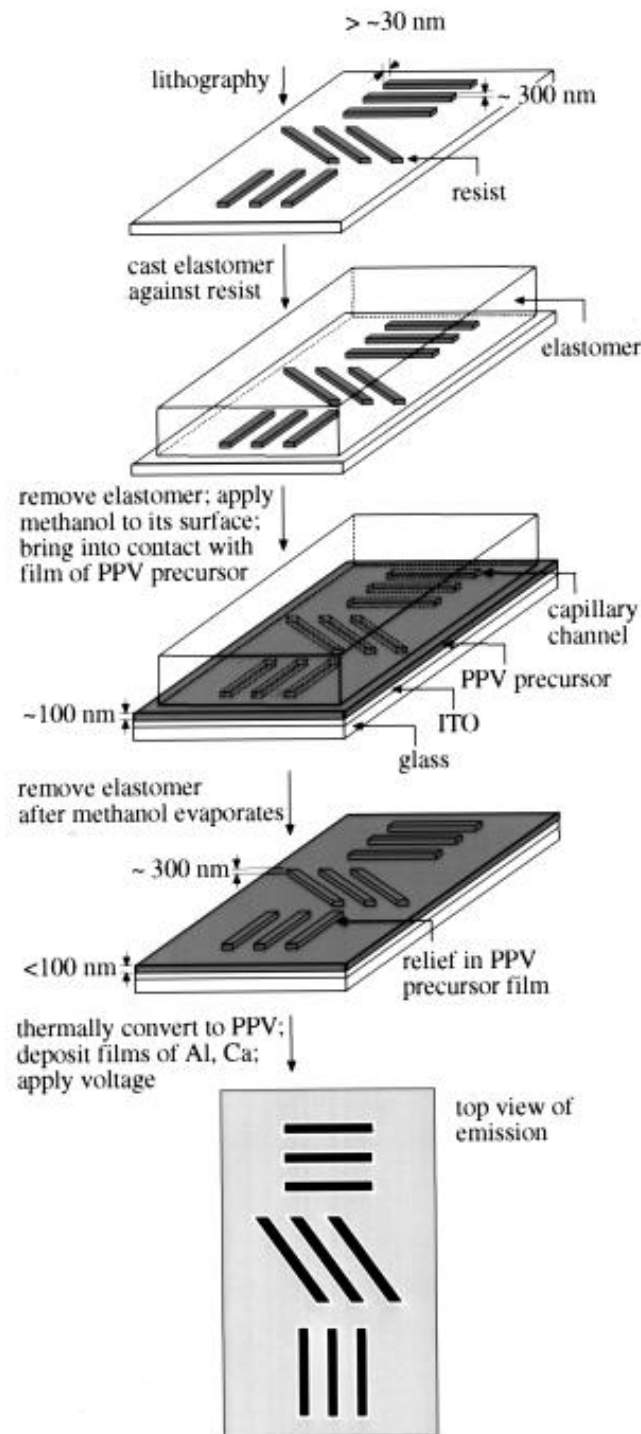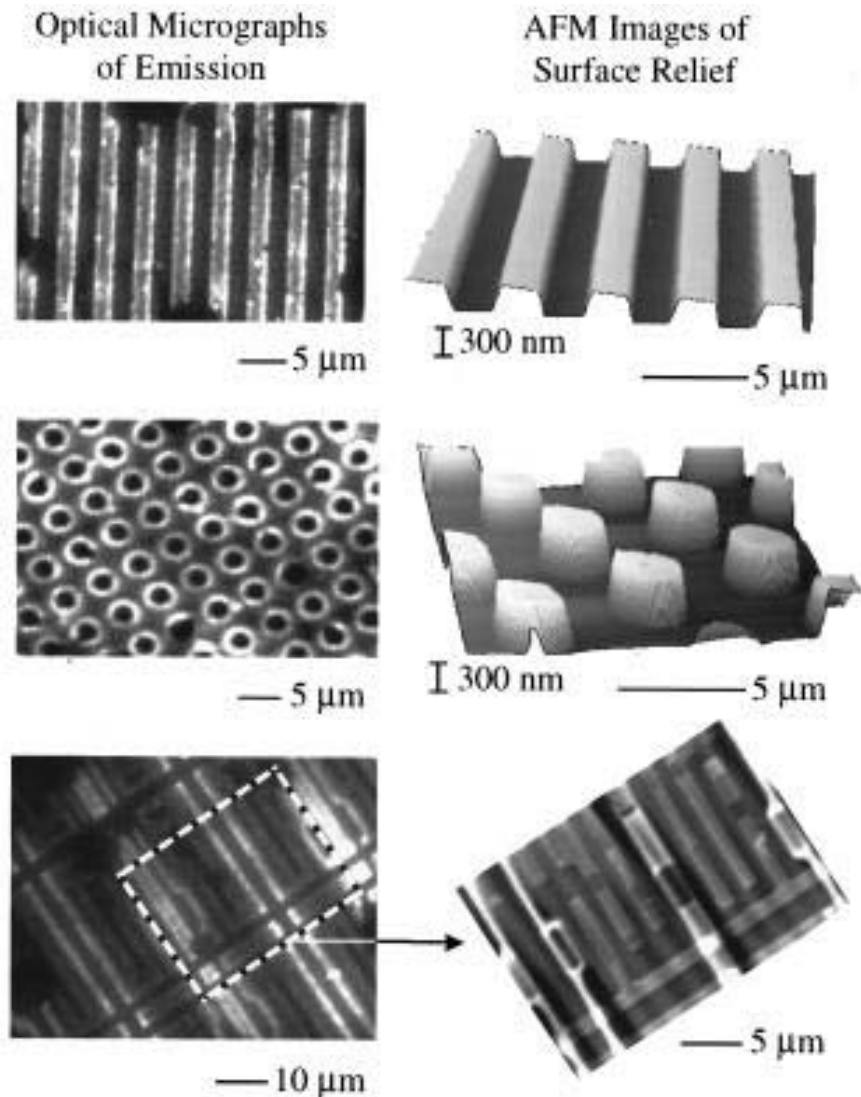
Left frames: Optical micrographs of emission from LEDs that incorporate structured films of PPV.
Right frames: AFM images of the surfaces of molded films of PPV.

Appl. Phys. Lett. 1998, **73**, 294
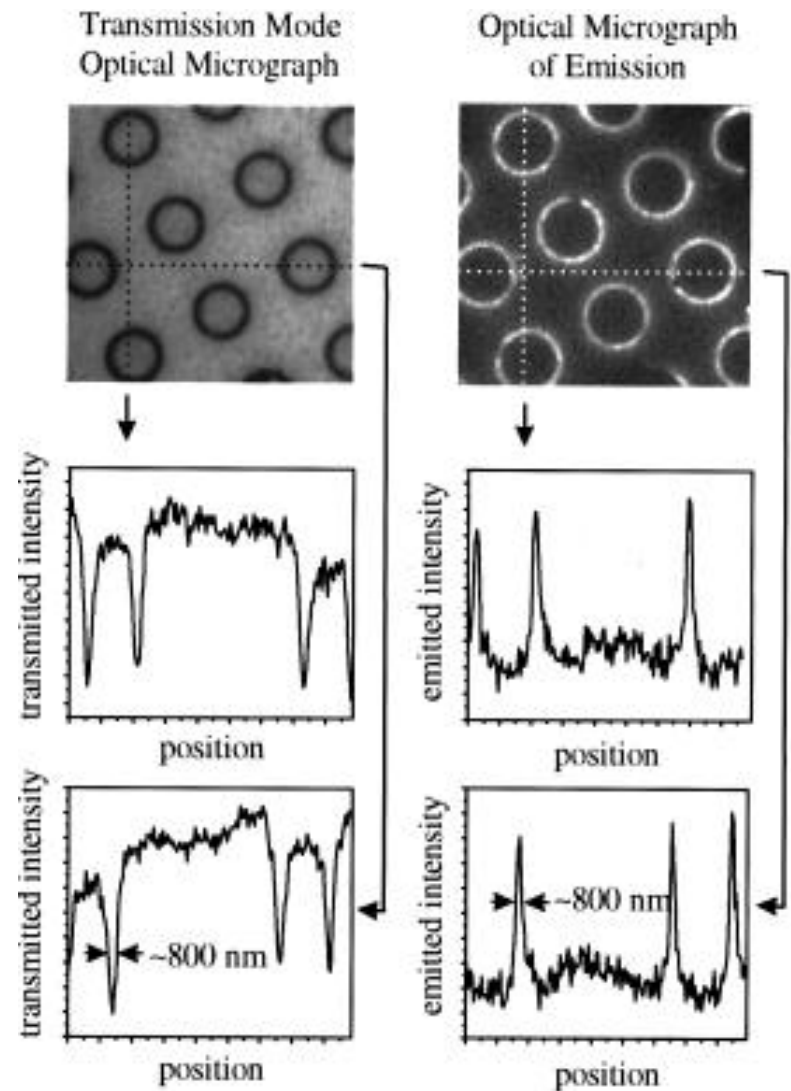
Left frames: Transmission mode optical micrograph and line graphs of the variation of intensity
Right frames: Optical micrographs of emission, and line graphs of the variation of the intensity

Replica Imprinting

(A) Master

(B) Polymer Replica

(C) Master

(D) Polymer Replica
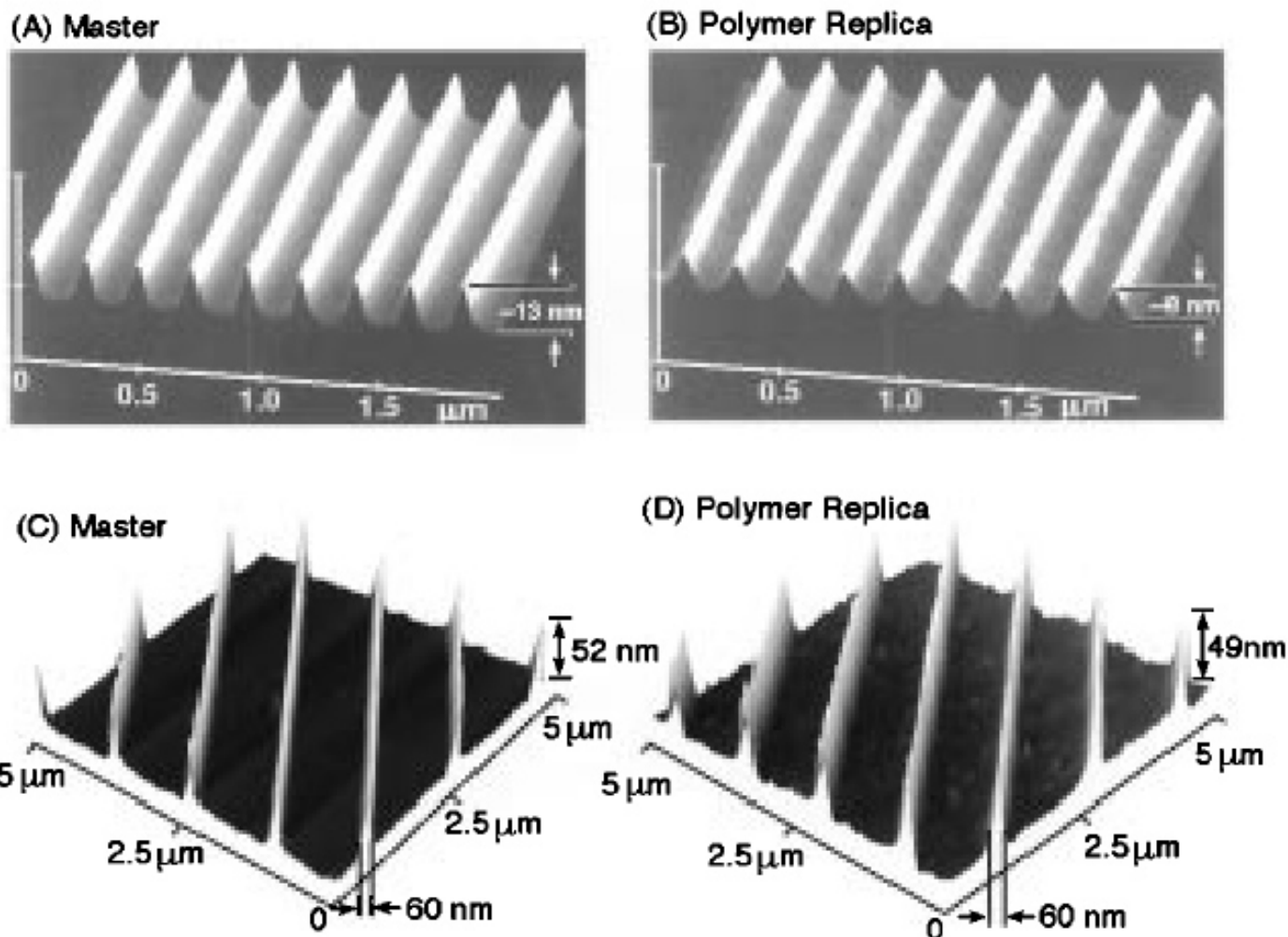
(A,B) AFM images of chromium nanostructures on a master, and a polyurethane replica prepared from a PDMS mold cast from this master. (C,D) AFM images of gold nanostructures on another master, and a polyurethane replica produced from different a PDMS mold cast from this master.[47]

Compression Replicas

Cross-sectional SEMs of the original master (generated in a photoresist film coated on a silicon wafer using photolithography) and the polyurethane replicas generated after different cycles of replication in PDMS, compression, and replication in polyurethane.[126,127]
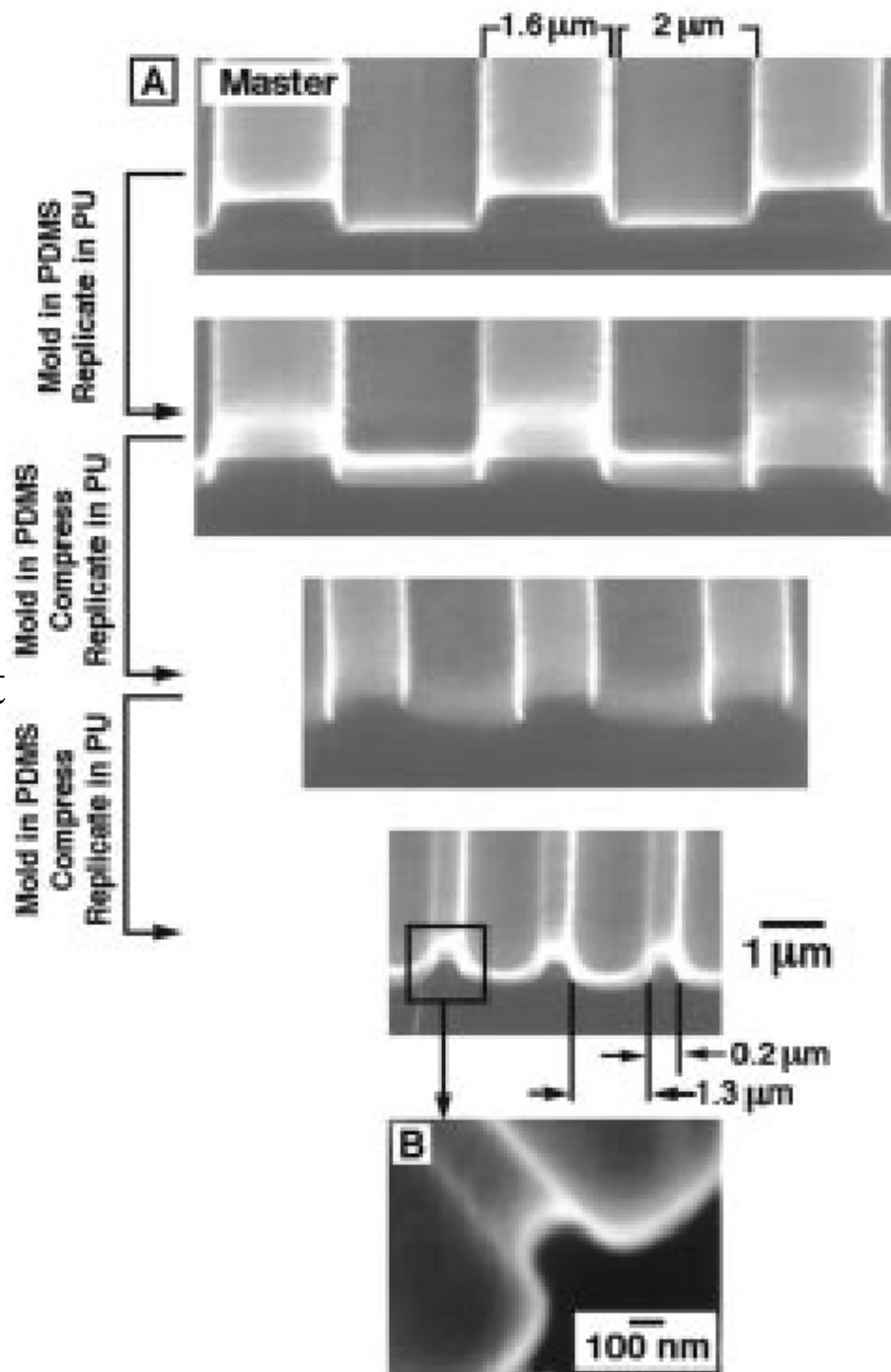
Microlens Projection Photolithography

(a) Optical system for microlens projection photolithography. A layer of photoresist coated on a substrate was placed
at the image distance from the microlens array.

(b) Fabrication of microlens arrays with aperture stops using reflow of melted
photoresist.

b) Coat photoresist on transparent, conductive glass substrate

Photoresist
glass
12-nm Au / 3-nm Ti

Fabricate an array of disks of photoresist

Photoresist
glass
12-nm Au / 3-nm Ti

Electroplate substrate with 200-nm copper

Photoresist
glass
Cu

Melt photoresist

Lenses
glass
Cu

Fabricate PDMS spacer

PDMS Lenses
glass
Cu

PDMS spacer
microlens
200-nm Cu aperture
glass substrate

a)

Si substrate
photoresist
PDMS spacer
$D = 2r$
microlens
metallic aperture
glass substrate

glass slide

r: radius of the lens;
S: sag height (thickness) of the lens;
f: focal length of the lens;
$n\_\_ \sim 1.4$;
$n\_\_ \sim 1.7$

Self-Assembly

Templating – Block Copolymers
1-D, 2-D and 3-D
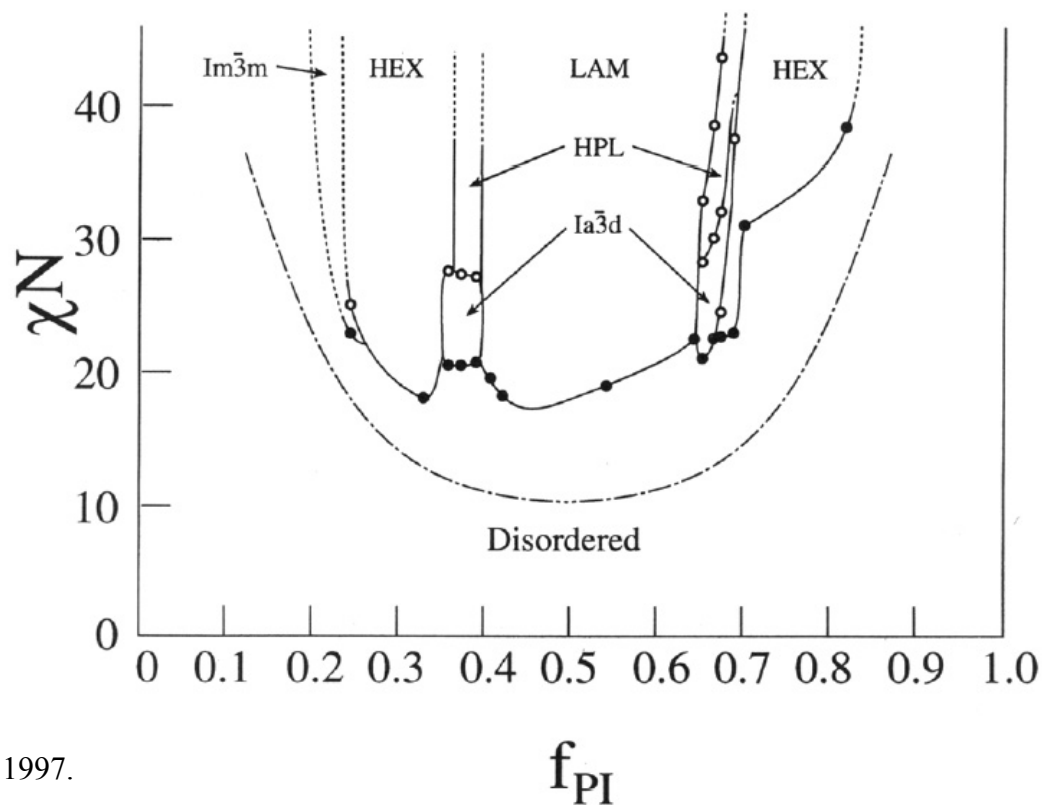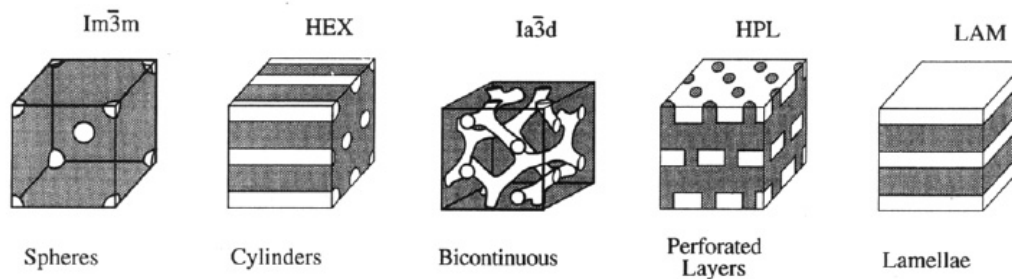
Nano-patterned Polymer Brushes

The structure of the block copolymer (left), schematic drawings showing a rod-coil diblock with a reactive hairy rod (center), and a magnified view of the Si-O linkages between a rod and a surface (right). Unlabeled lines from the oxygen atoms designate the bonds to the Si substrate. Many linkages exist between a rod and the substrate because the number of triethoxysilyl groups in a rod is equal to the degree of polymerization of the PIC rod.
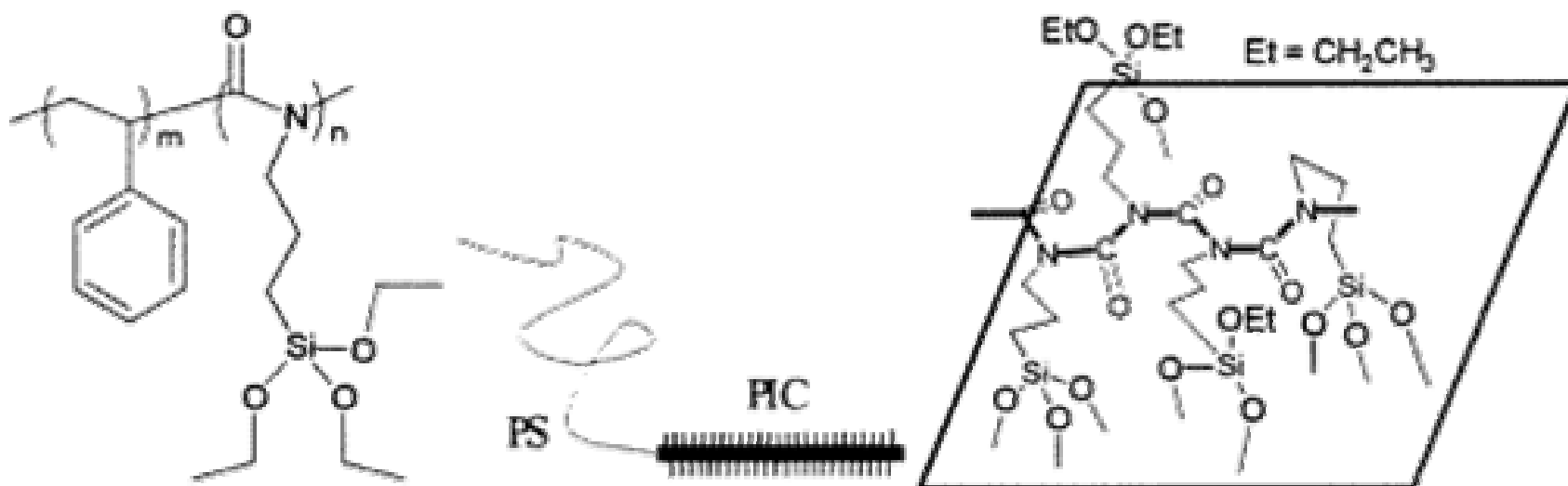
Nano-patterned Polymer Brushes

Tapping mode AFM height images for the rod-coil brush prepared on Si wafers immersion-coated from block copolymer solution in toluene (300 mg/mL):

(a) plane view and   (b) side view (1.0 × 1.0 m²).

(a)

(b)

20 nm
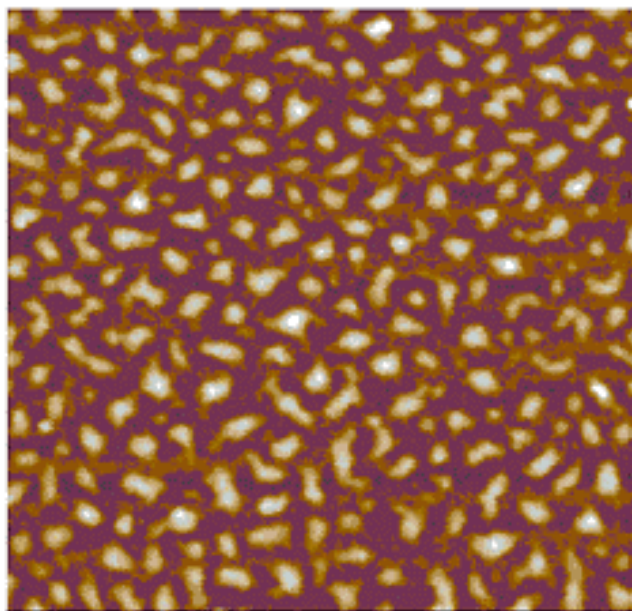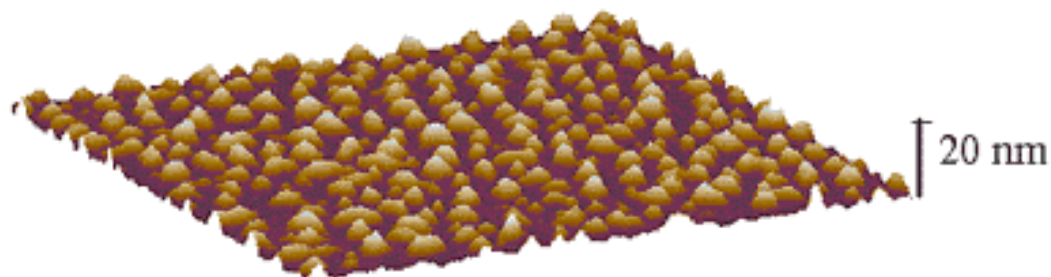
Nano-patterned Polymer Brushes

AFM height images of the rod-coil brush patterns prepared by contact printing:
(a) $50 \times 50 \ \mu m^2$ and (b) $10 \times 10 \ \mu m^2$. In part b are shown a height profile and a magnified area ($2 \times 2 \ \mu m^2$) with an inset showing the Fourier transformed image.

15 nm

0   50(μm)

(a)

0   10 (μm)

0   2 (μm)
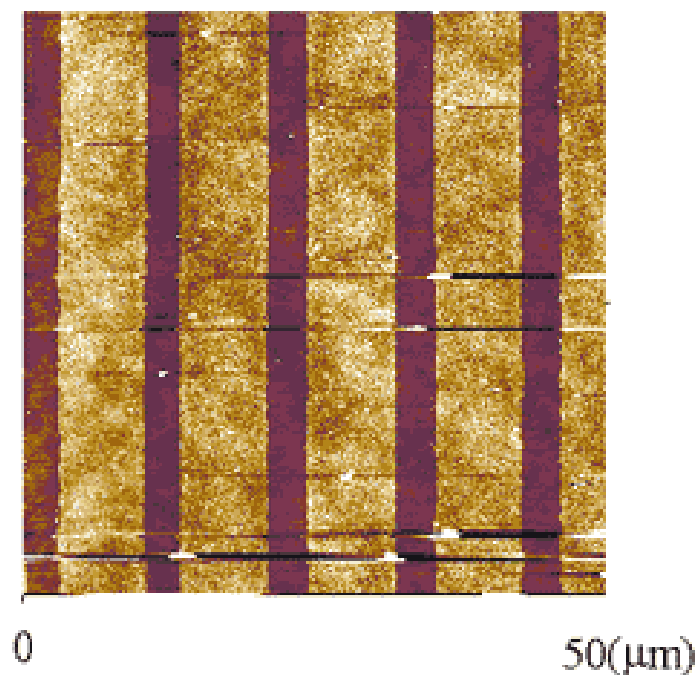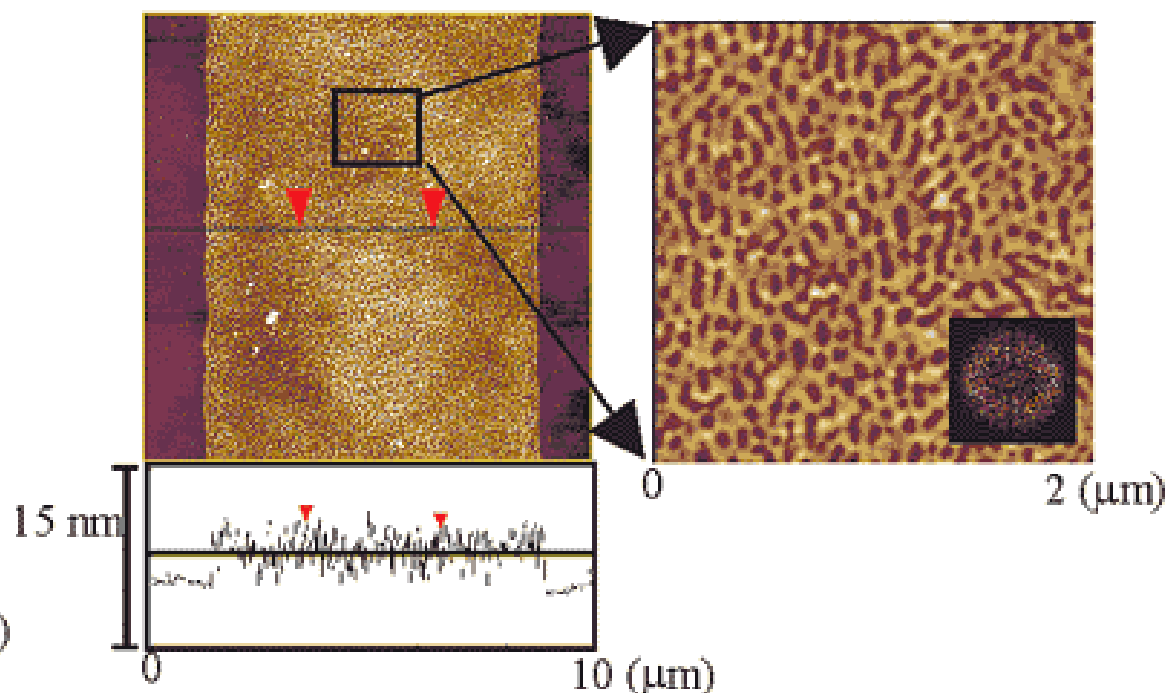
(b)

Nanopattern Diblock Copolymer Films

Plan-view TEM image of a free-standing monolayer film of PS-P4VP micelles. The P4VP block was selectively stained with I_2 and appeared as dark spherical cores. Inserted is a Fourier transformed pattern of the boxed area.
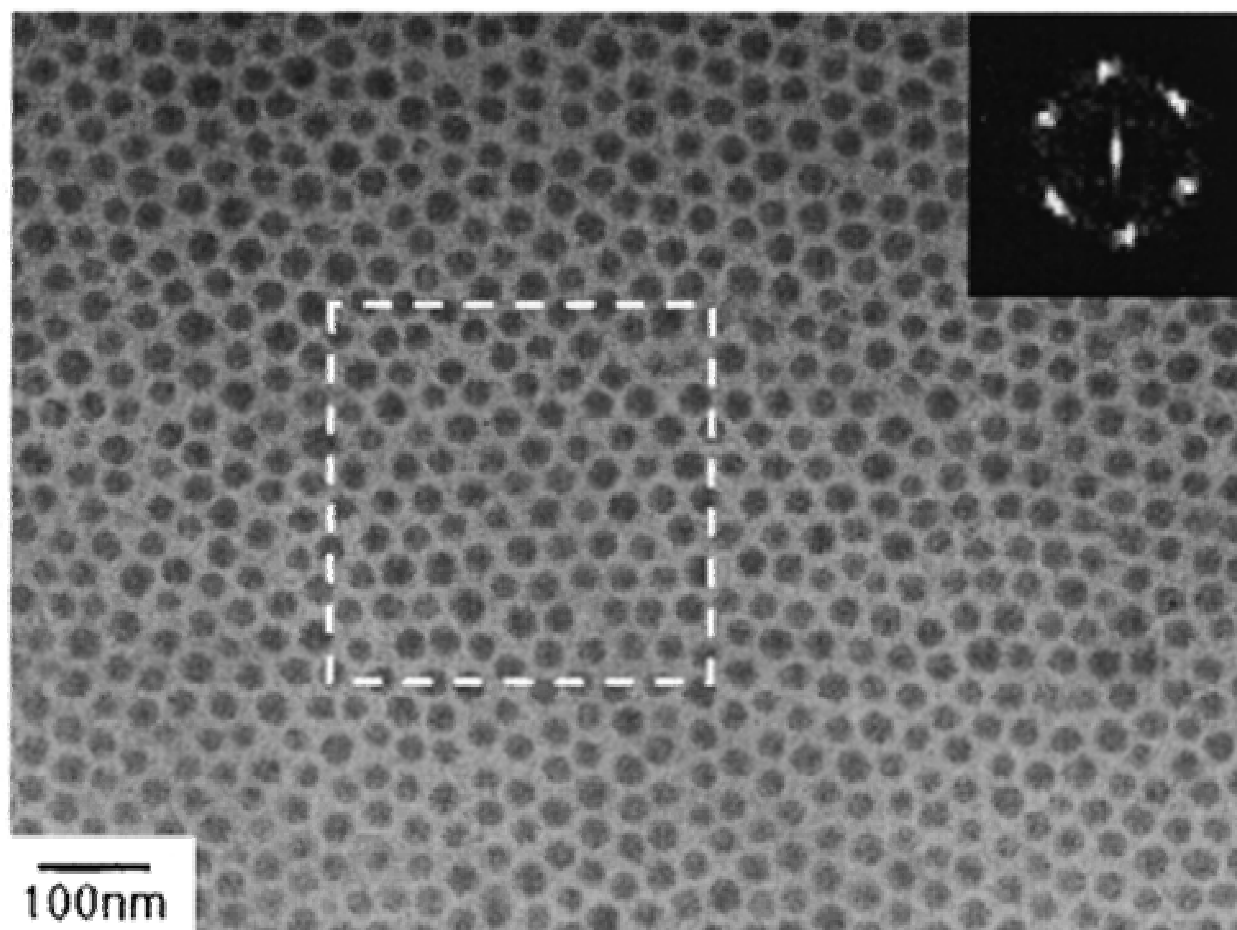
Nanopattern Diblock Copolymer Films

Plan-view TEM image of a free-standing monolayer film of PS-P4VP micelles after in situ core-corona inversion. The P4VP block was again selectively stained with I_2 and appeared as a dark continuous matrix.
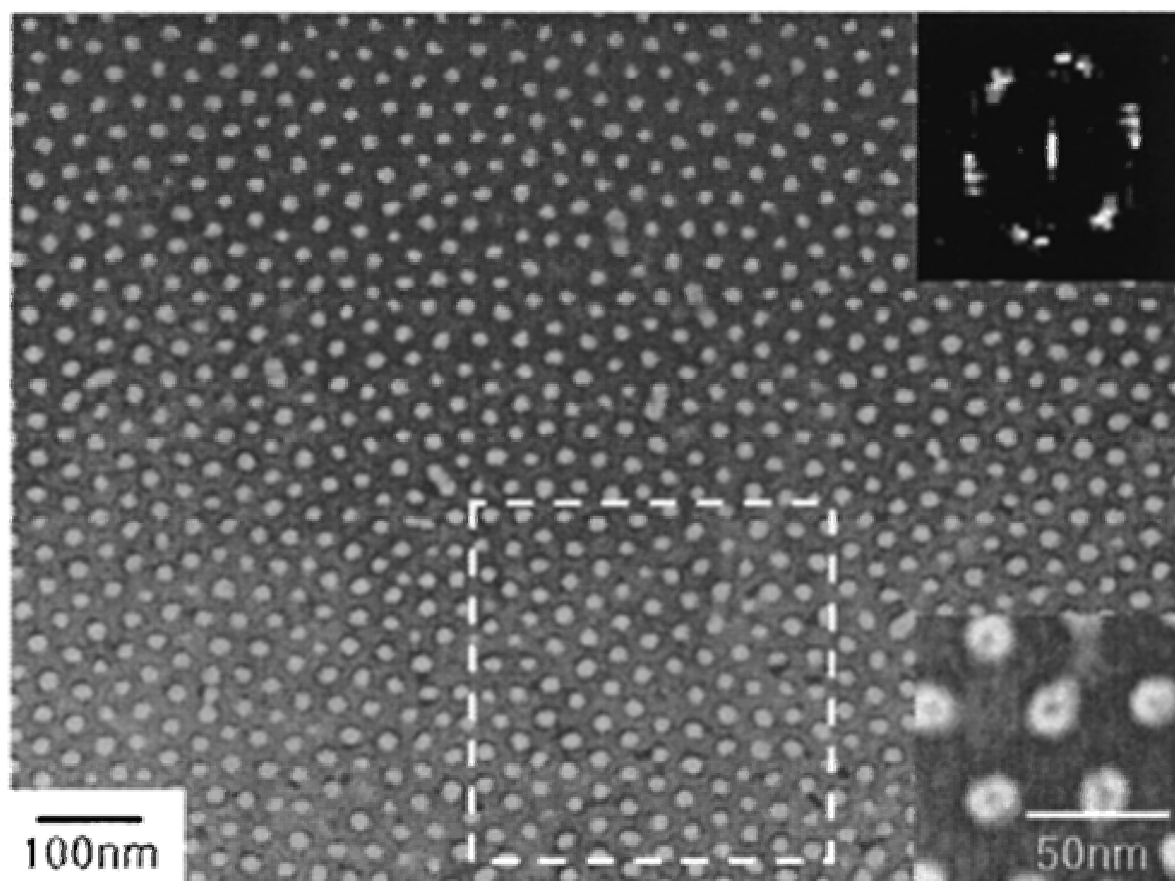
Nanopattern Diblock Copolymer Films

Plan-view TEM images of monolayer films of PS-P4VP micelles containing electron-beam-reduced silver nanoparticles

(a) before and   (b) after in situ core-corona inversion.
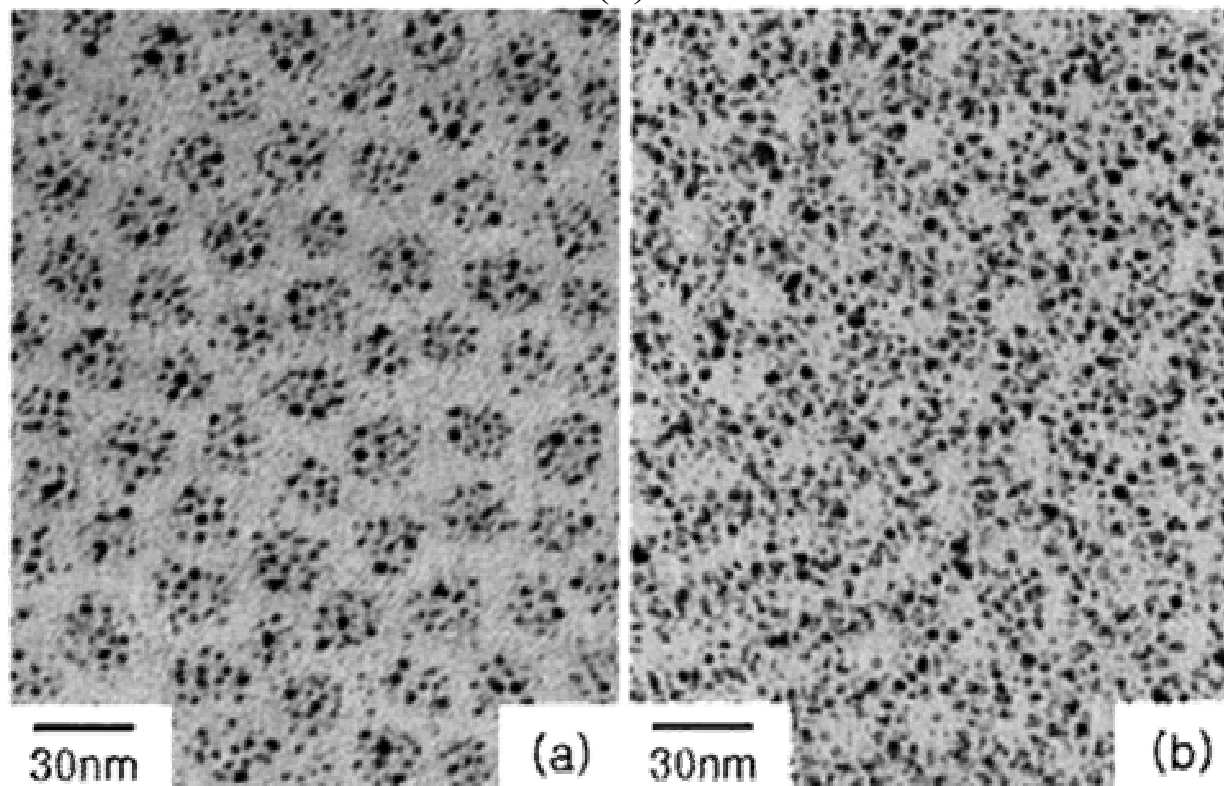
Nanoscale Templated Polypyrrole Patterns

AFM (topology) images of the evolution of Ppy (Polypyrrole) deposition on LB films of PS-P4VP as a function of polymerization reaction time: LB film (a) before Ppy deposition and (b) after 60 min of Ppy polymerization. Each LB film was formed on a freshly cleaved mica substrate. Image size: 1μm × 1μm.
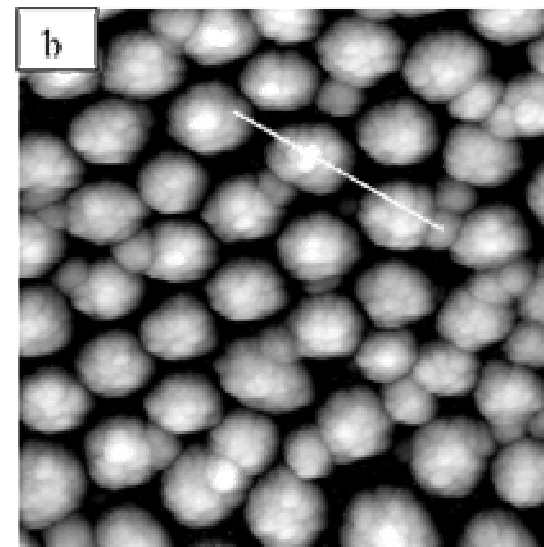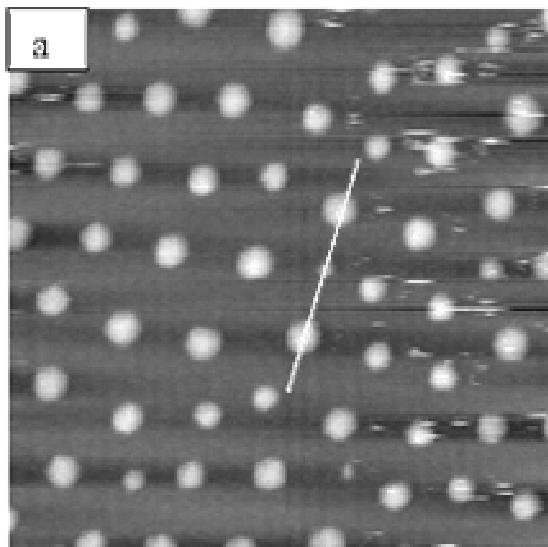
Ppy growth has been shown to be kinetically preferred on hydrophobic vs hydrophilic surfaces
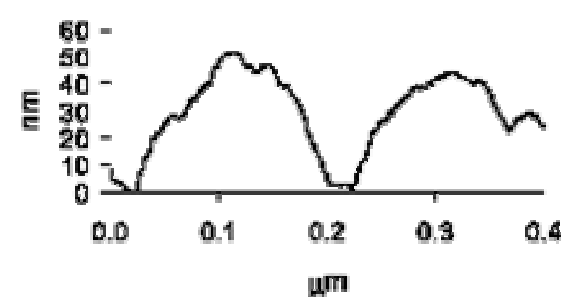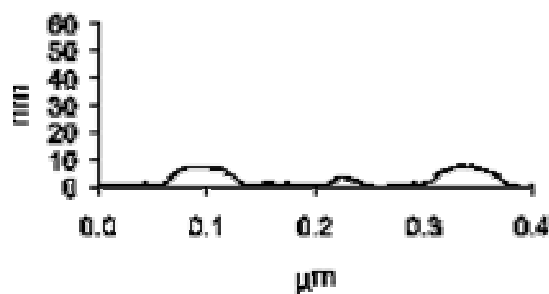
Nanoscale Templated Polypyrrole Patterns

AFM (topology) images of the evolution of Ppy deposition on SA films as a function of polymerization reaction time: SA film (a) before Ppy deposition, (b) after 30 min of Ppy polymerization, and (c) after 150 min of Ppy polymerization. Each SA film was formed on a freshly cleaved mica substrate. The apparent lack of periodicity in the 1D line scan in (b) is caused by the fact that the topology of the Ppy is superimposed on the topology of the underlying SA film. Image size: 1 μm × 1 μm.
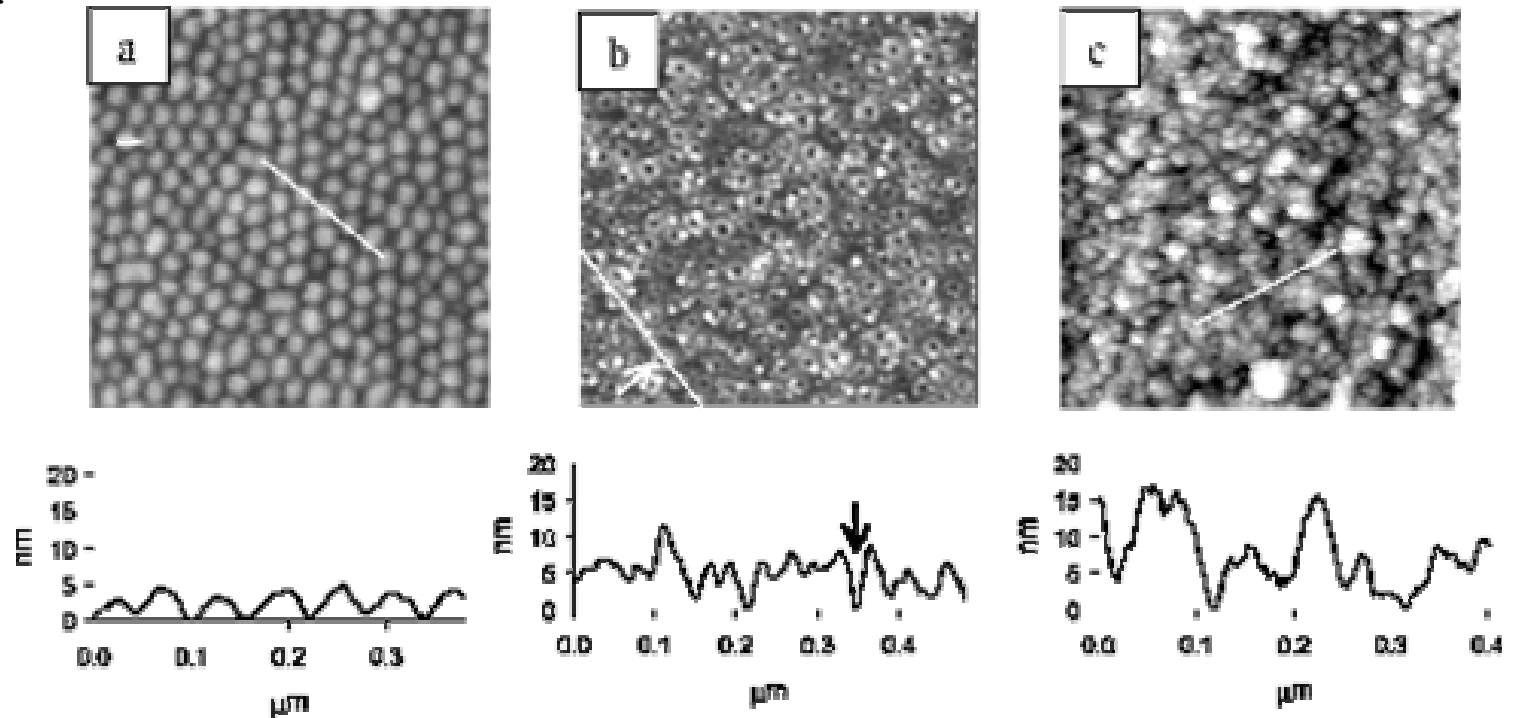
Block Copolymer Lithography

(**A**) Schematic cross-sectional view of a nanolithography template consisting of a uniform monolayer of PB spherical microdomains on silicon nitride. PB wets the air and substrate interfaces.

(**B**) Schematic of the processing flow when an ozonated copolymer film is used, which produces holes in silicon nitride.

(**C**) Schematic of the processing flow when an osmium-stained copolymer film is used, which produces dots in silicon nitride.
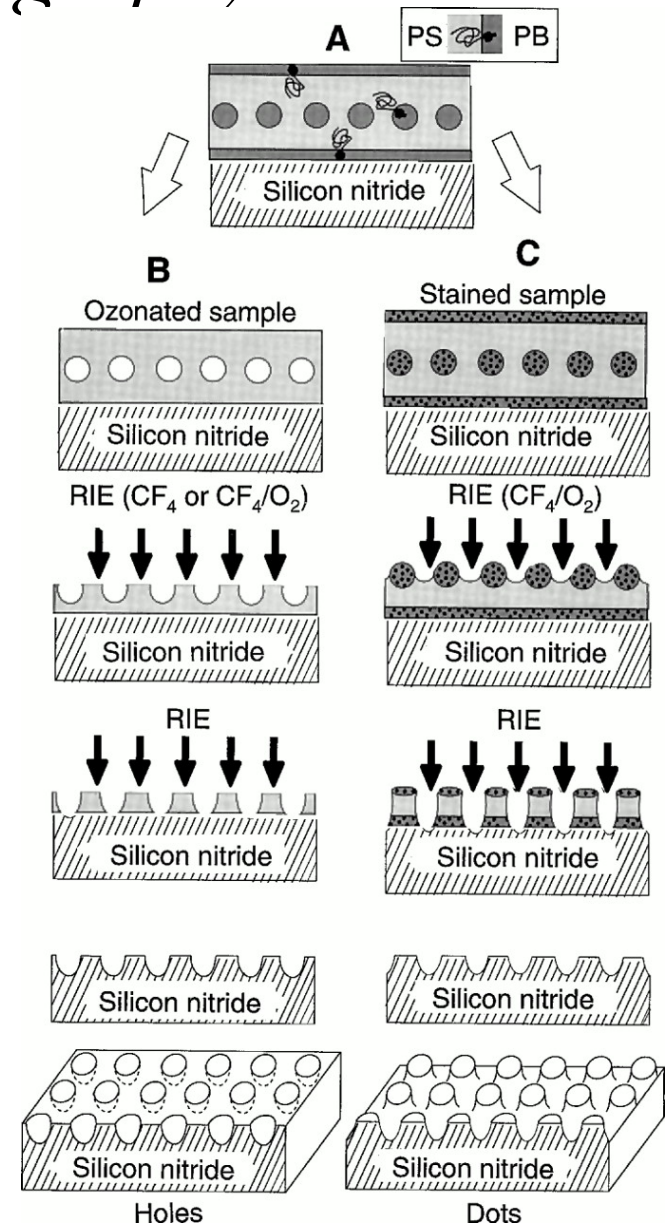
Block Copolymer Lithography

A series of TEM micrographs showing film processing. (**A**) A spherical microdomain monolayer film before RIE. The lighter regions are the PB domains that were degraded and removed by ozonation, and the darker background is the PS matrix. (**B**) Hexagonally ordered arrays of holes in silicon nitride after RIE. The pattern was transferred from a copolymer film such as that in (A). The lighter regions are ~15-nm-deep holes that were etched out. (**C**) A cylindrical microdomain monolayer film before RIE. The darker lines are osmium-stained PB cylinders that lie parallel to the surface. (**D**) Fingerprintlike lines in silicon nitride after RIE. The pattern was transferred from a copolymer film such as that in (C). The darker regions are ~15-nm-thick ridges in the silicon nitride, which were protected from RIE.
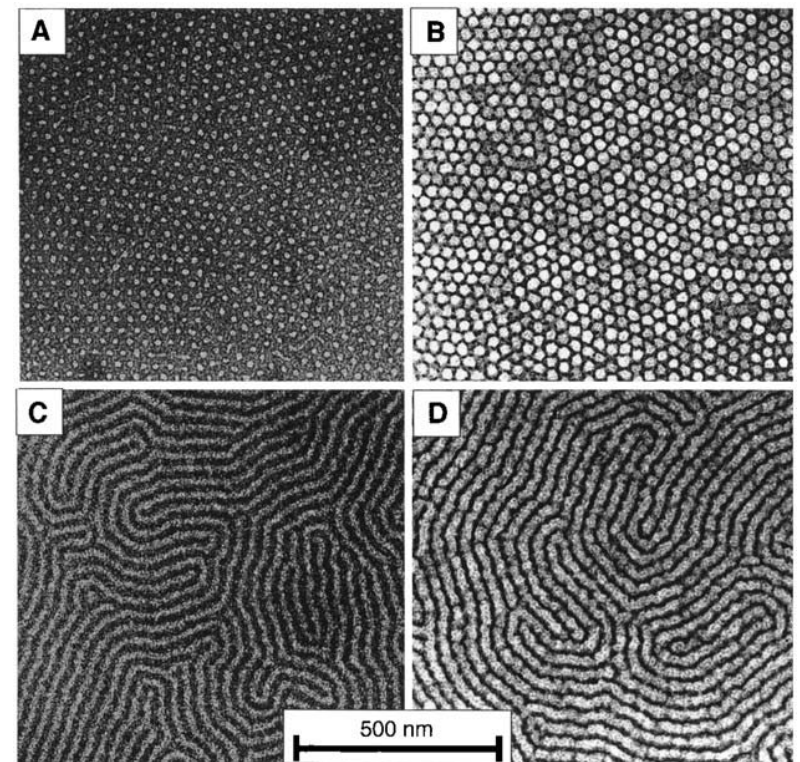
Self-assembly Nanosphere Lithography

Highly ordered monolayer of polystyrene nanospheres (diameter 0.5 m) on Si substrate made by the self-assembly nanosphere lithography.

(a) AFM image of the closely packed hexagonal nanospheres,

(b) single blue color of the area 10×10 mm^2,

(c) FFT showing the high quality of the array.
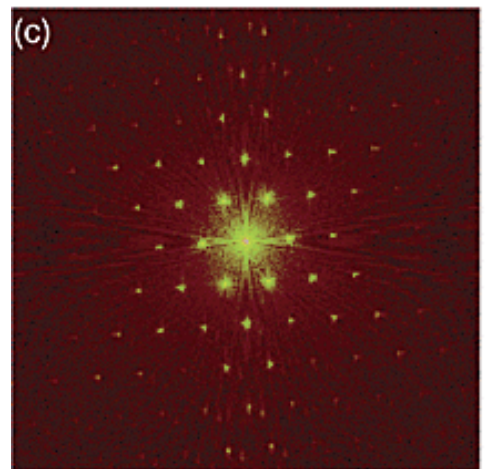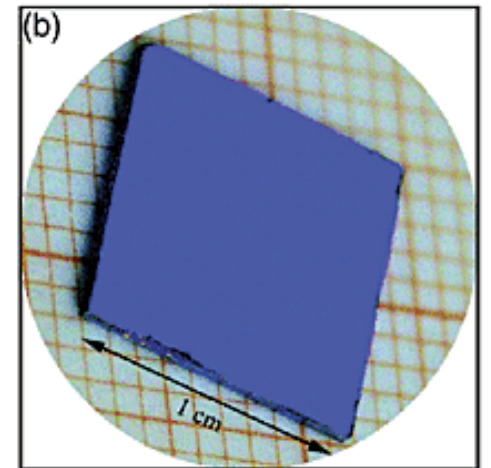
Self-assembly Nanosphere Lithography

AFM and SEM images of the Ni dots made by nanosphere lithography.

(a) AFM image of the Ni dots made from the nanospheres,

low (b) and

high (c) magnifications of the round Ni dots after annealing at 900 °C in vacuum for 1 h.
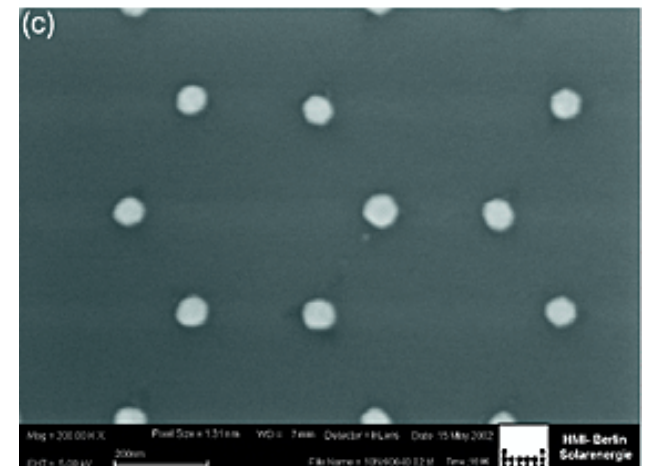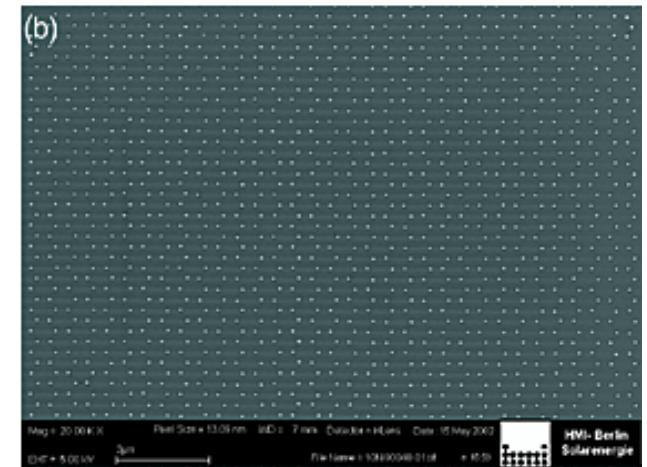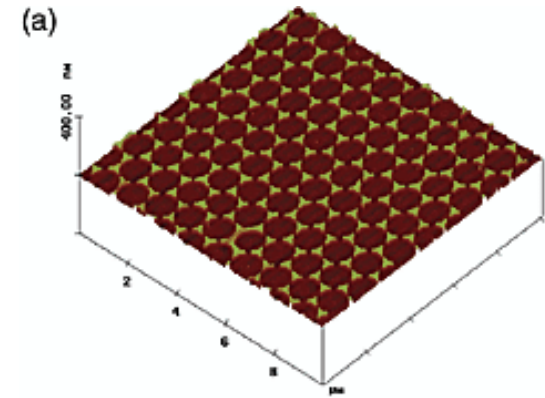
Self-assembly Nanosphere Lithography

Low (a) and

high (b) magnification SEM images of the highly ordered honeycomb array of aligned carbon nanotubes grown by PECVD,

(c) bright diffraction colors of red, blue, and green.
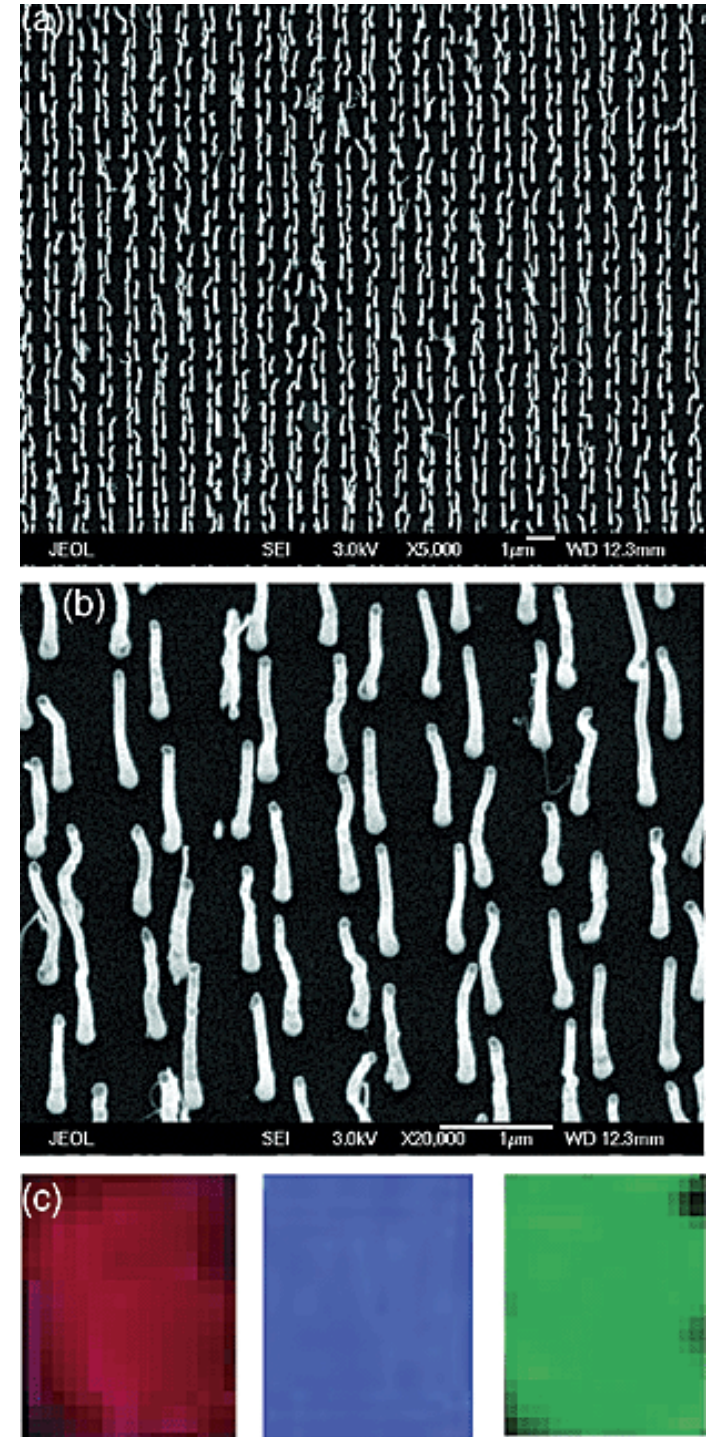
Dip-Pen Nanolithography

TMAFM (Tapping ModeAFM) topographic images (A, C)
and SEM image (B) of an etched MHA (16-
mercaptohexadecanoic acid) /Au/Ti/ SiO_x/Si dot nanoarray.
The insets are high-resolution images.

Hierarchical Sphere Self-assembly

Pack column with beads; fill in and cure polymer

Allow bead-containing rods to self-assemble; fill small gaps between rods with polymer; cure

Dissolve beads

Remove polymer matrix

Fill in other material

Hollow spheres
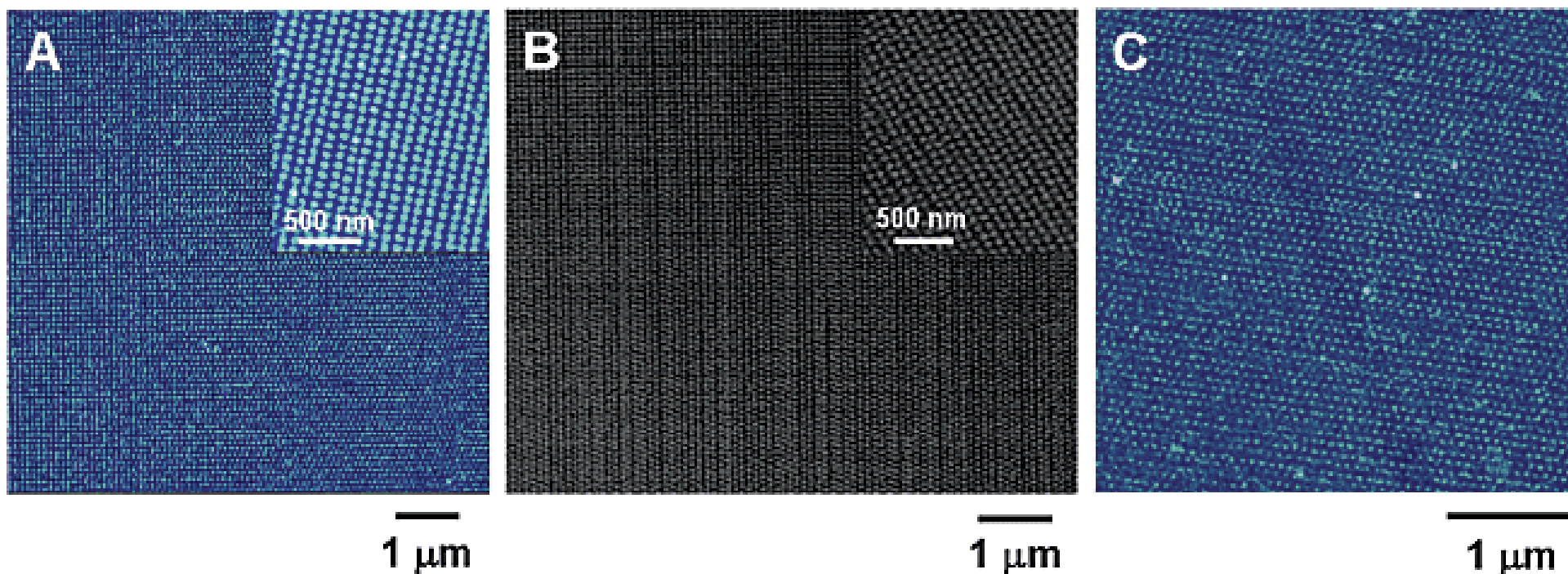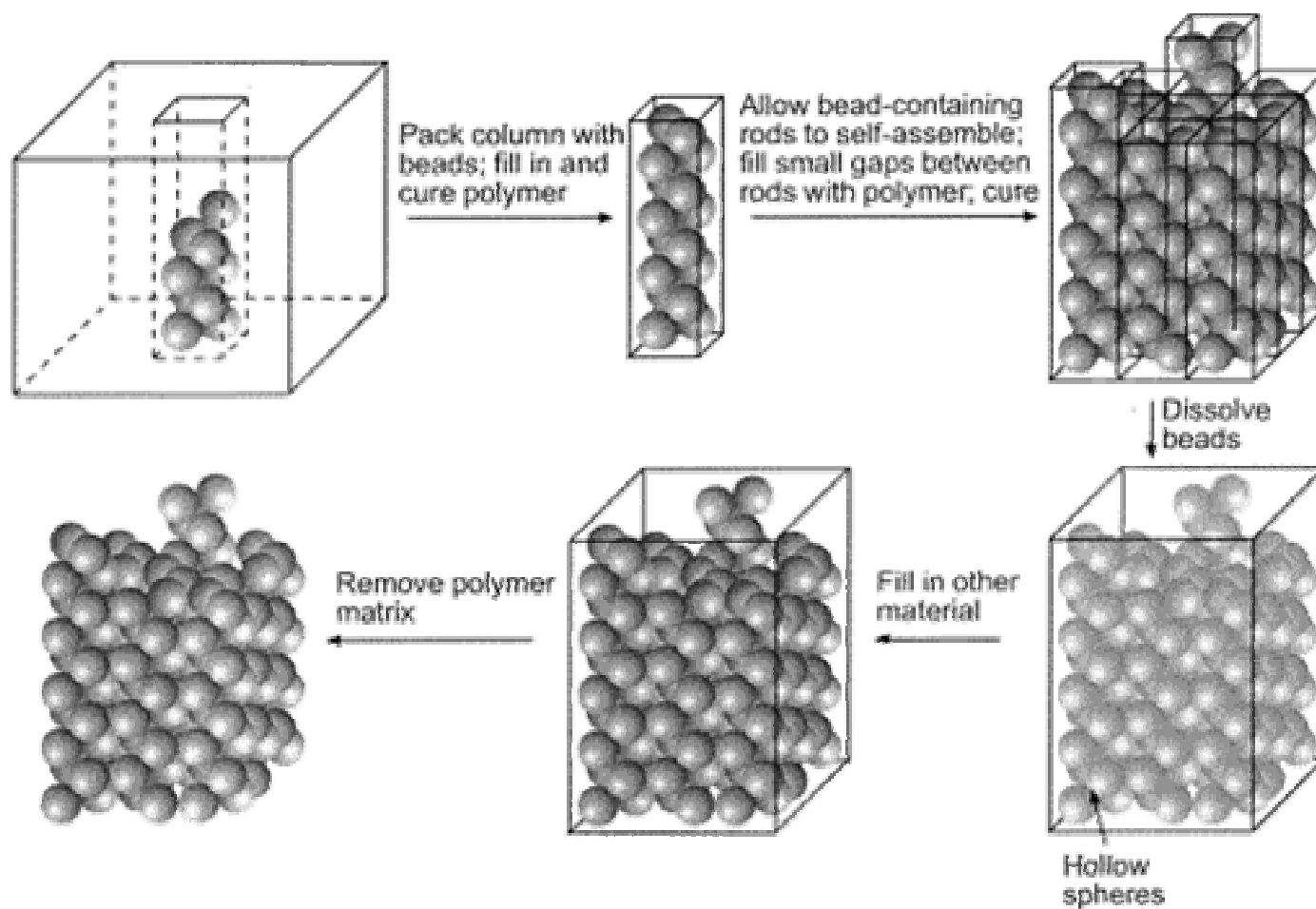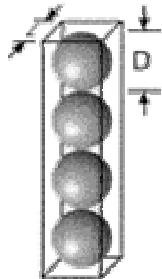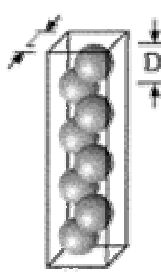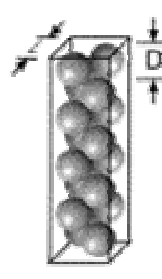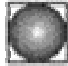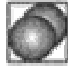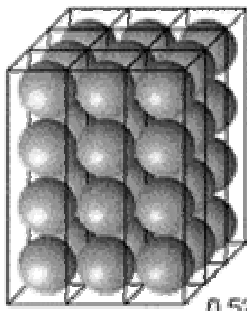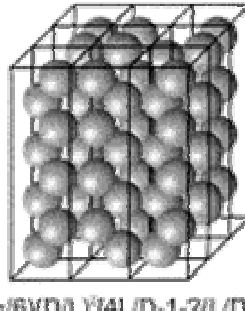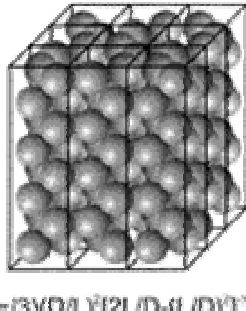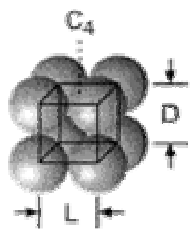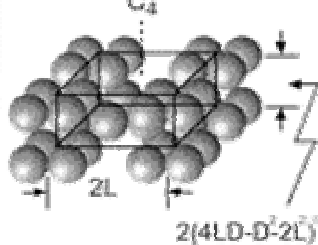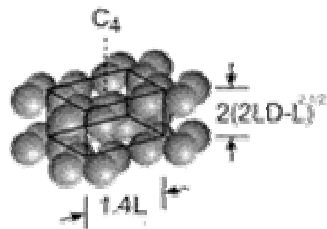
Hierarchical Sphere Self-assembly

Beads pack into square columns in different ways as their size (relative to the size and shape of the column) changes from 1.00 to 0.59 (diameter of bead, D/side of square, L). The structure resulting from self-assembly of these bead-containing rods changes from a simple cubic lattice to a body-centered-tetragonal lattice over this range.

Other properties-the filling factor of the solid by the spheres and the dimension of the lattice-also change

D/L	1	$0.59 < D/L < 1$	$0.5 < D/L < 0.59$
Sphere packing in a single well			
Top view of packed well			
Side view of packed well			
Self-assembly structure (filling factor)	0.52	$(\pi/6)(D/L)^2[4L/D-1-2(L/D)]^{-1/2}$	$(\pi/3)(D/L)^2[2L/D-(L/D)]^{-1/2}$
Bravais lattice	Simple cubic	Body-centered tetragonal	Body-centered tetragonal
Unit cell	C_4; D; L	C_4; $2L$; $2(4LD-D^2-2L^2)^{1/2}$	C_4; $2(2LD-L^2)^{1/2}$; $1.4L$

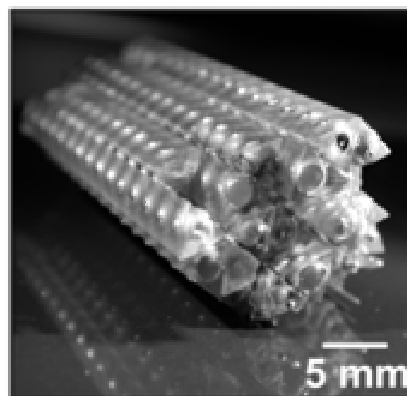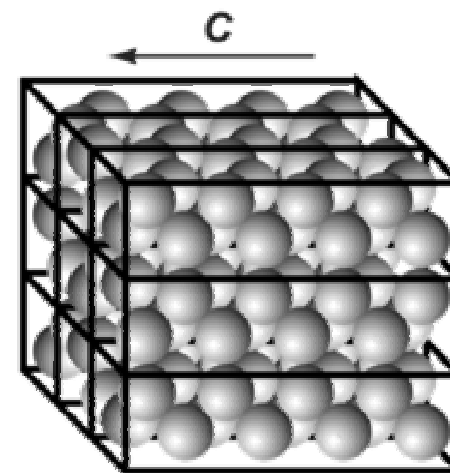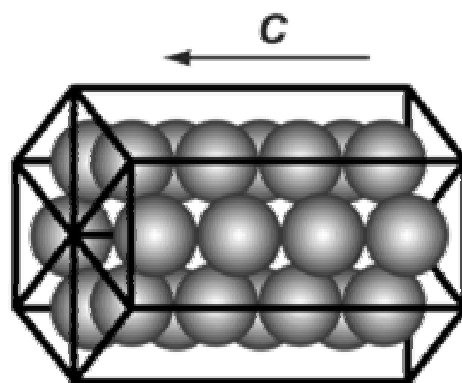# Hierarchical Sphere Self-assembly
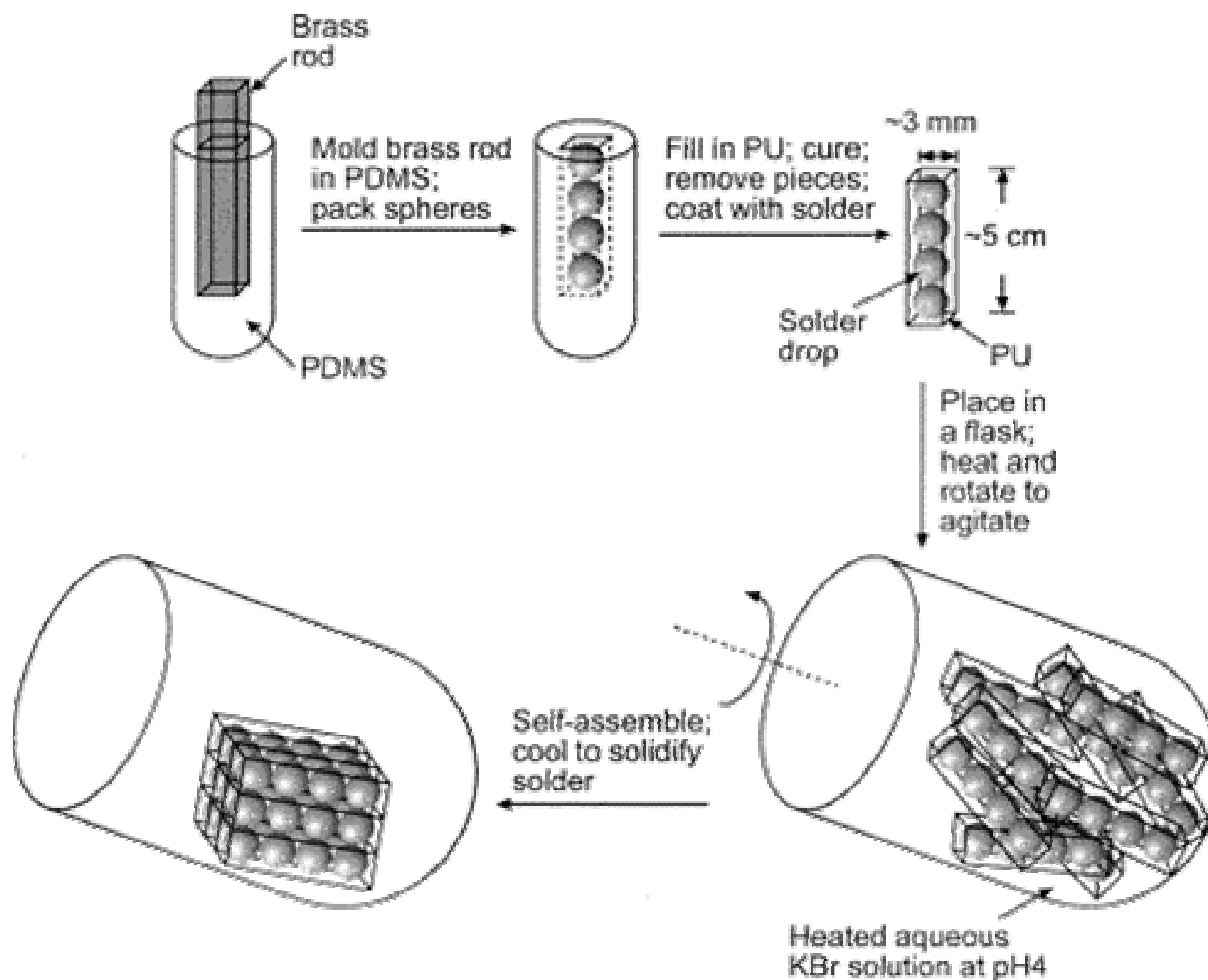
Schematic procedure used to pack spheres in columns and to allow self-assembly of these columns in a heated aqueous KBr solution at pH 4.

Hierarchical Sphere Self-assembly
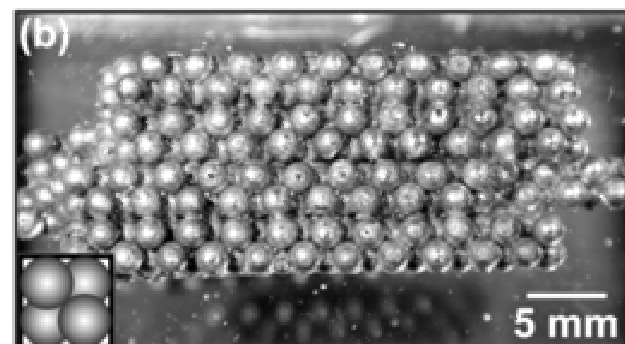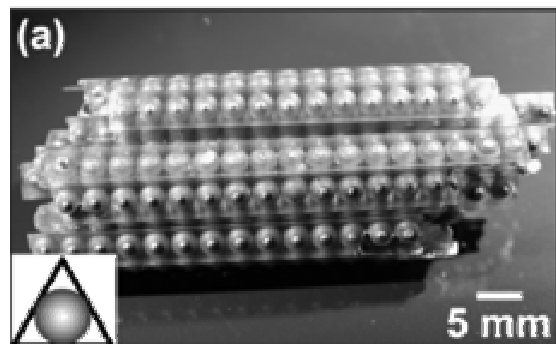
(a) Left column: a self-assembled hexagonal lattice of metal-coated, polymer beads.

(b) Right column: a self-assembled body-centered-tetragonal lattice of polymer beads. For both columns, the top photographs are the side view of the self-assembled structures (the insets are schematic top view of packed columns); the middle ones are the schematic illustration of the structures; and the bottom photographs are the top view of the structures
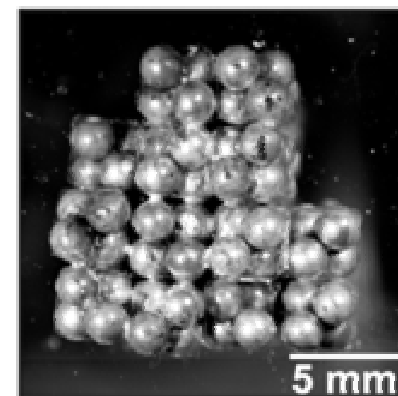
Hierarchical Sphere Self-assembly

Template effect of the container on the self-assembly of rods.
(a) Schematic outline of self-assembly in a container that
acted as a template for the final, desired structure.
(b) Photograph of a self-assembled simple-cubic lattice of
brass beads.
(c) Photograph of a PDMS structure generated by dissolving
the brass beads and solder in the structure shown in (b);
(d) Photograph of a simple-cubic lattice of epoxy beads
formed by filling and curing epoxy in the structure shown in
(c), and removing PDMS; a few beads were removed on the
top layers to examine the inner structure.

In (b), (c), and (d), an inset shows the details of each
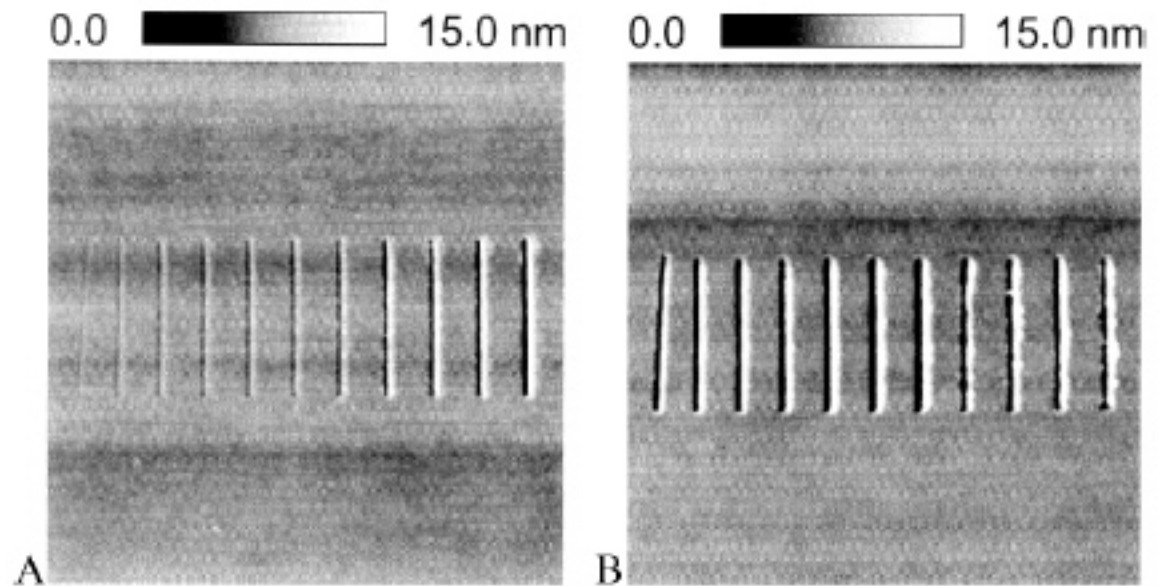structure.
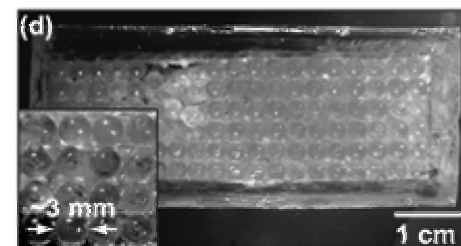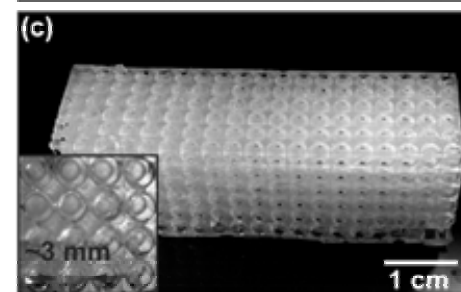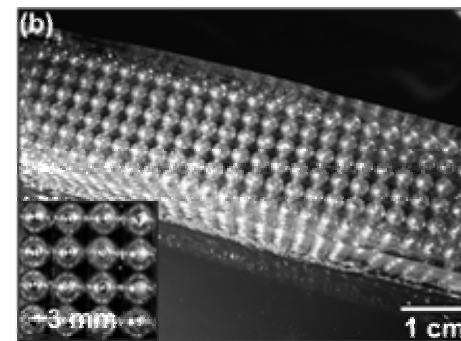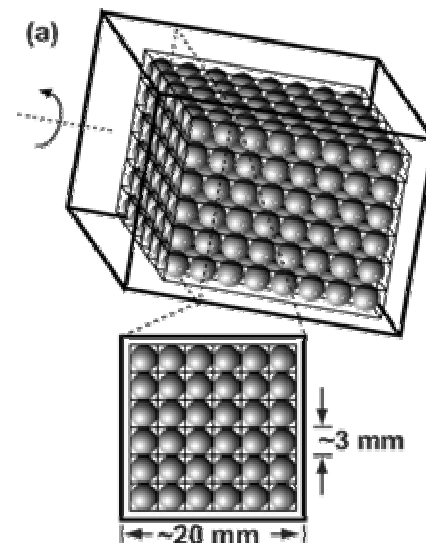
Direct Write

AFM Ploughing

Schematic fabrication of a nanoscale line with an AFM: ploughing of a furrow into a thin resist layer with the vibrating tip, A; subsequent etching of a groove and removing of the masking layer, B.
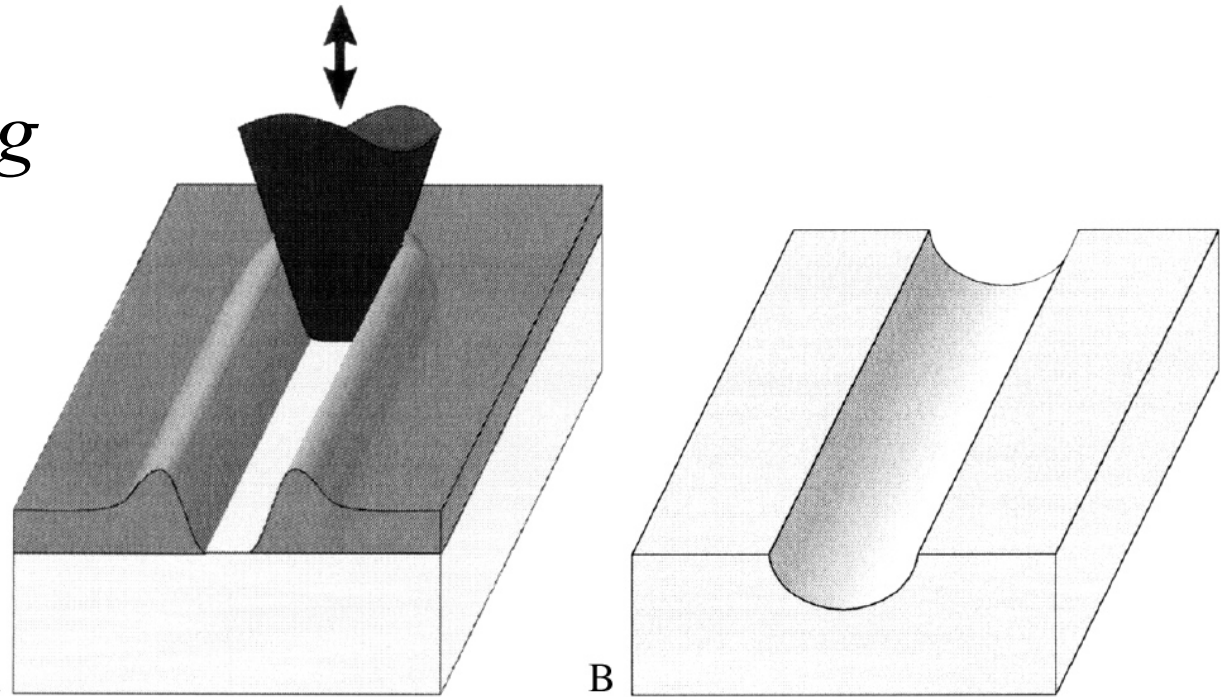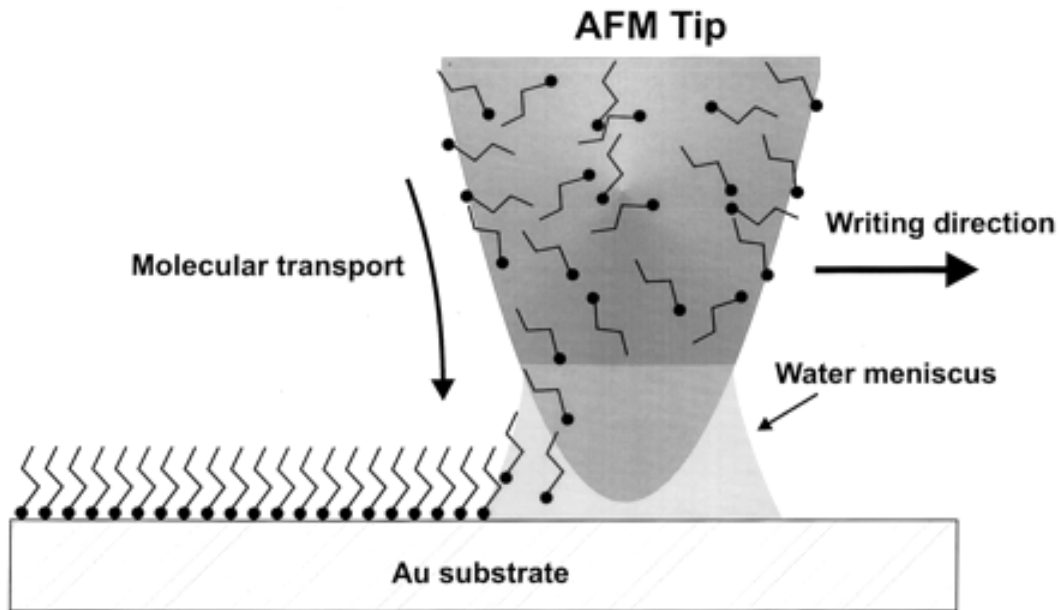
(Bottom); "Ploughing" enhancement factor via tapping – 6-15 times that of imaging

A

B

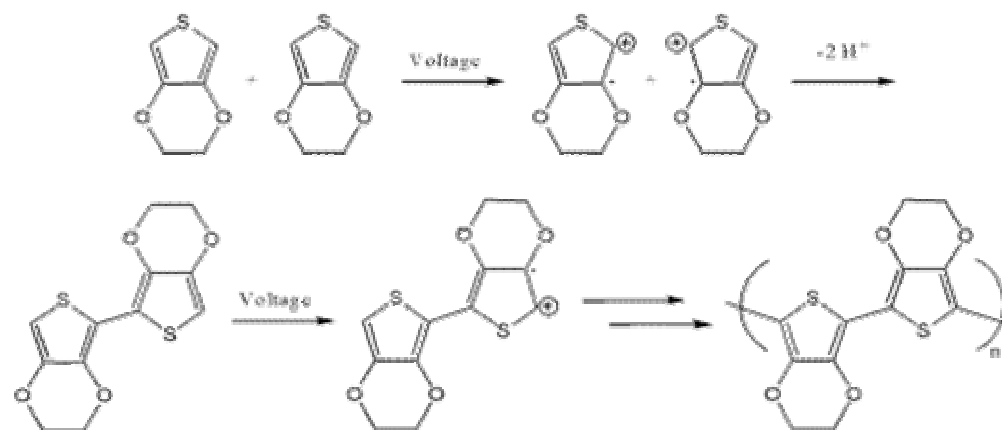| 0.0	15.0 nm

0.0	15.0 nm

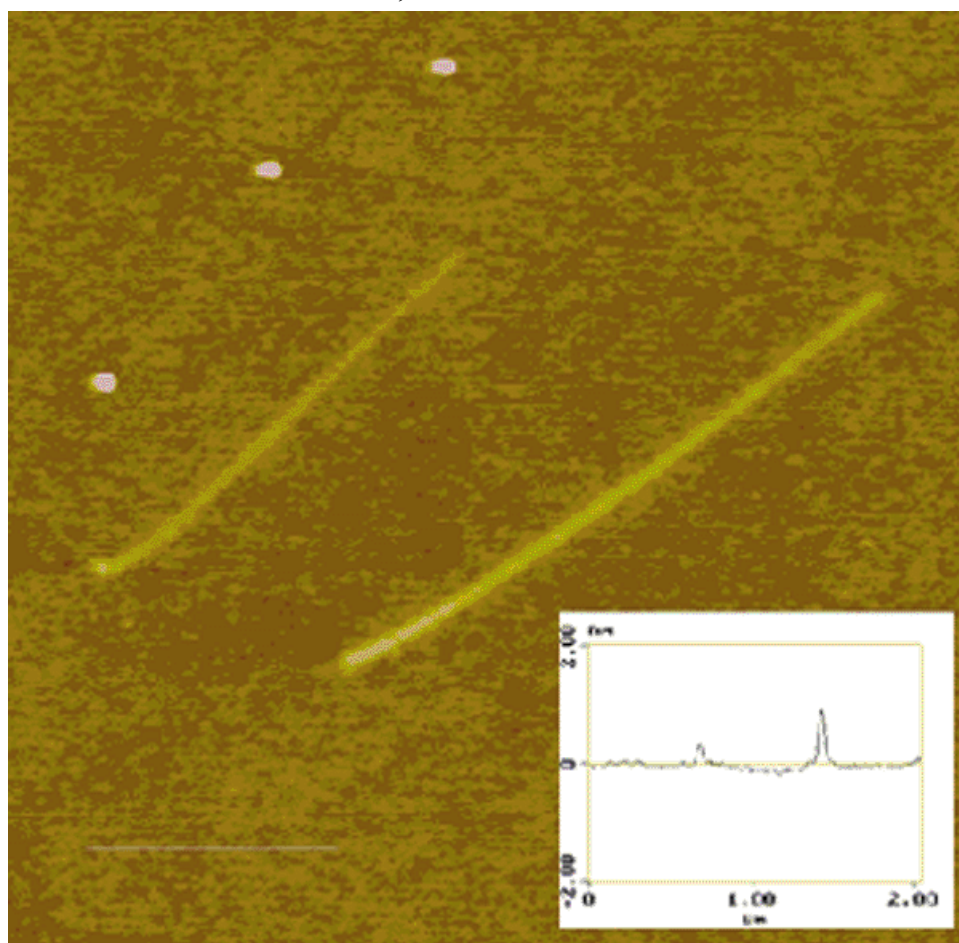A

B

Templating – 1-D

Dip-Pen Nanolithography

Schematic representation of DPN. A water meniscus forms between the AFM tip coated with ODT and the Au substrate. The size of the meniscus, which is controlled by relative humidity, affects the ODT transport rate, the effective tip-substrate contact area, and DPN resolution.
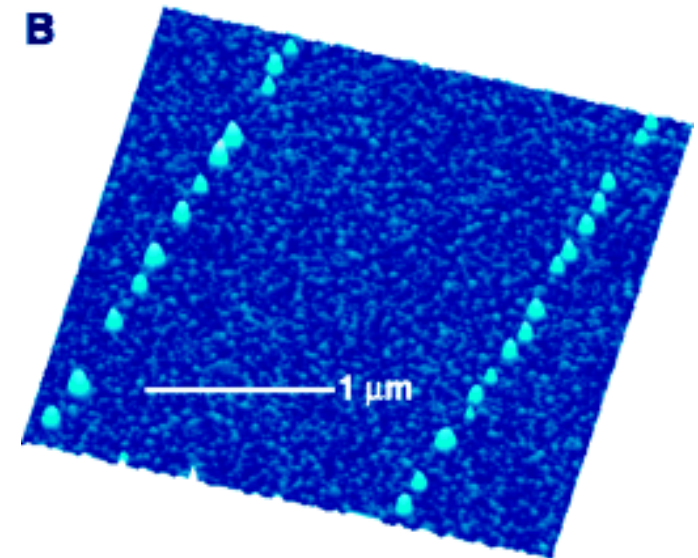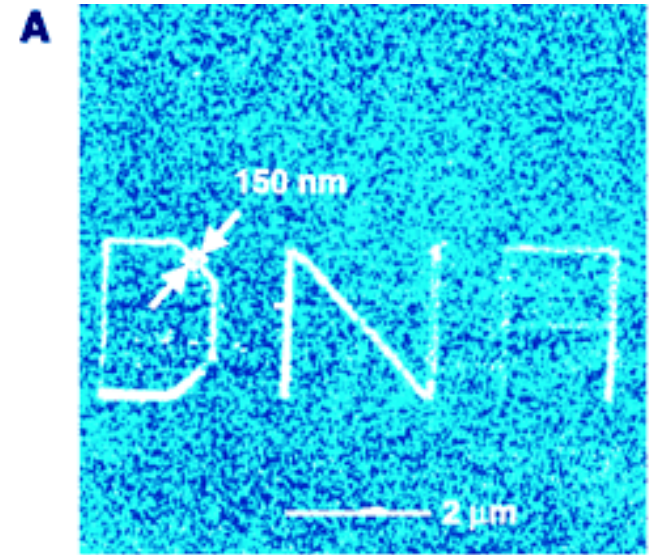
Polythiophene Nanowires

Oxidative Polymerization
Mechanism of Poly-EDOT

Two polymer lines written
(electrochemical dip-pen lithography)
at 10 (left) and 1 nm/s (right). The
humidity was 28% and the voltage was
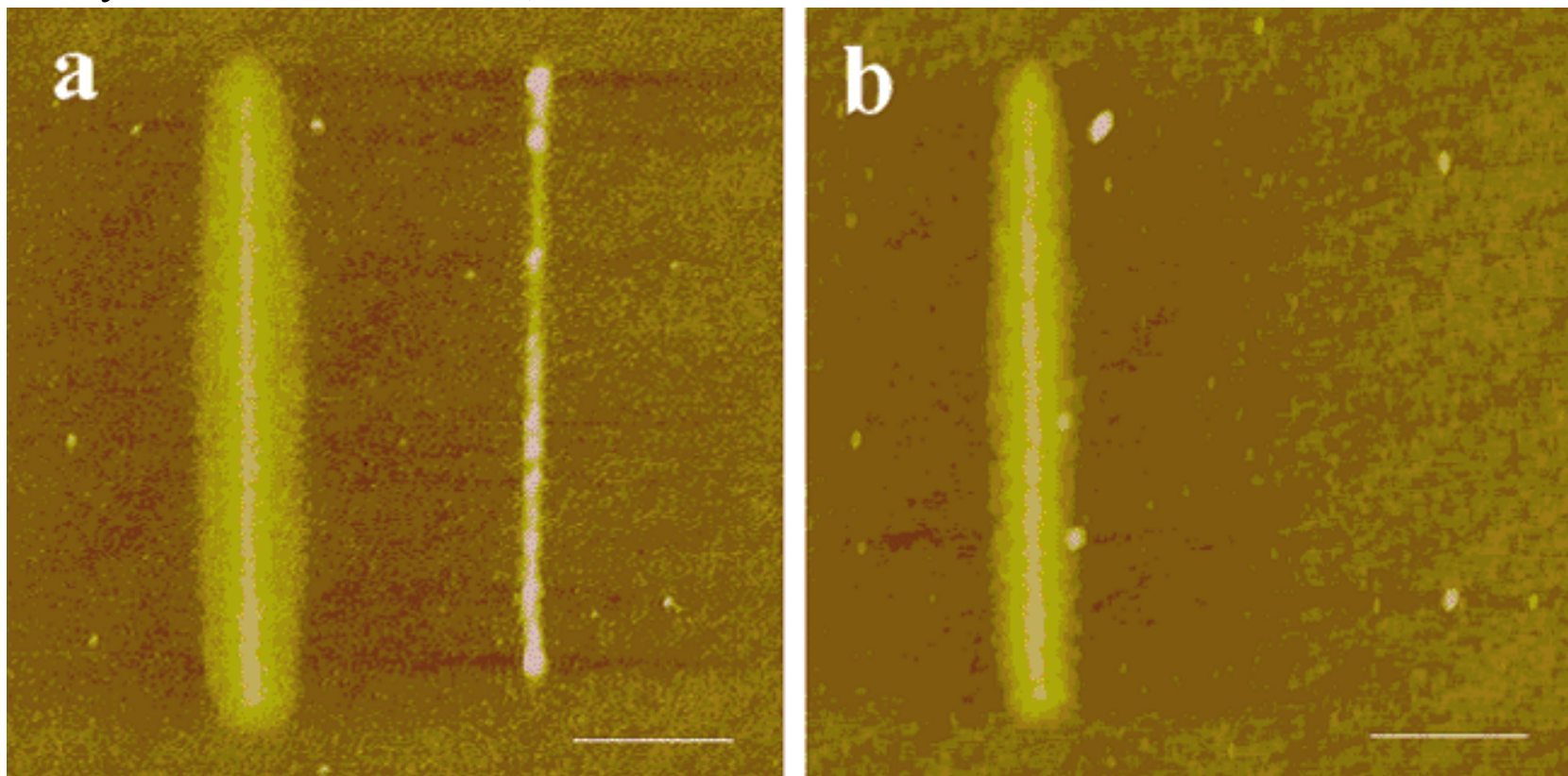-12 V. Polymer line width: 50 nm

scale bar: 1 μm.

Inset: Cross-section of the two lines.

Polythiophene Nanowires

SiO$_2$ (left-hand line) and polymer (right-hand line) features (a) before and (b) after chemical oxidation with 2:1 H$_2$SO$_4$:H$_2$O$_2$.

The polymer line was fabricated at 10 nm/s, 48% humidity, -12 V.

Polymer line width: 30 nm; scale bar: 250 nm.

Luminescent Dip Pen Lithography

(A) Scanning confocal microscopy image of a series of MEH-PPV polymer nanowires fabricated on glass surface.

(B) Plot of average fluorescence intensity of a polymer wires in (A) versus probe translation speed used to fabricate the wires.

(C) Lateral force image of a series of lines written on gold surface using mercaptohexadecanoic acid solution as ink.

(D) Plot of average line thickness for the alkanethiol lines on (C) versus probe translation speed used to fabricate these lines.
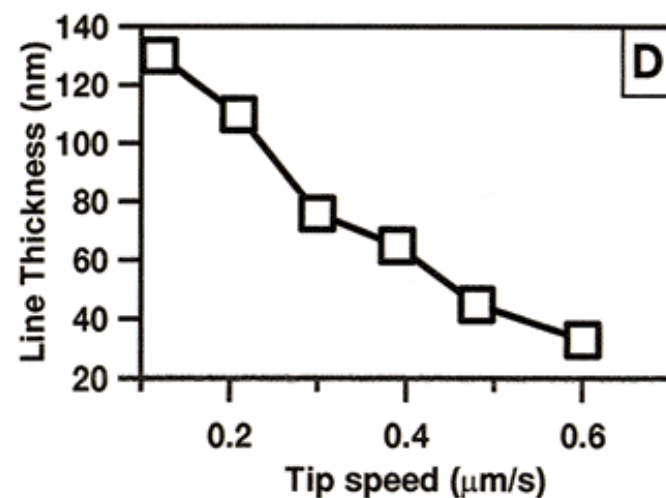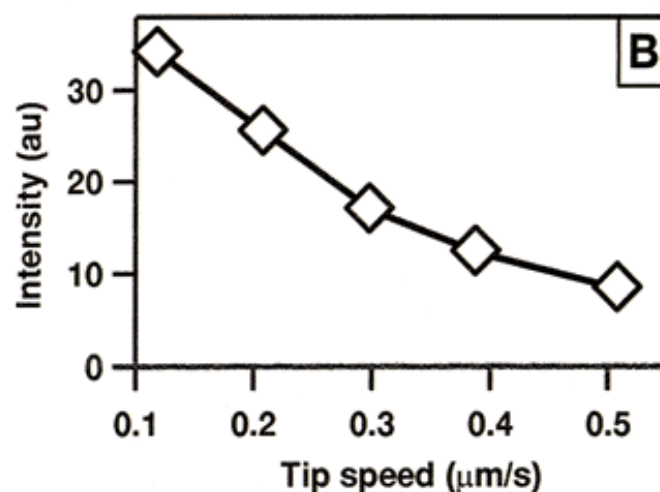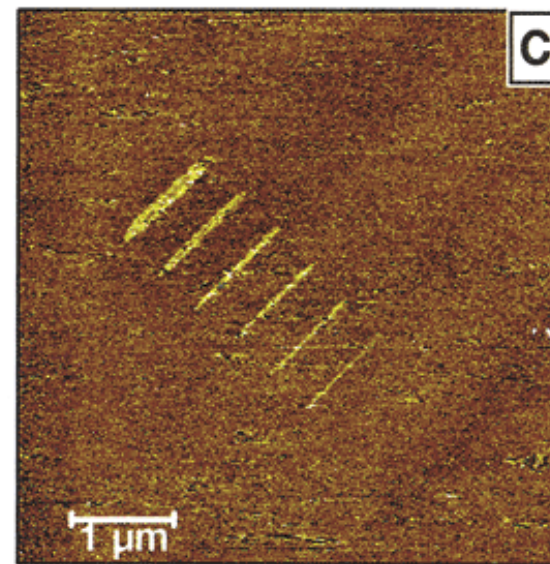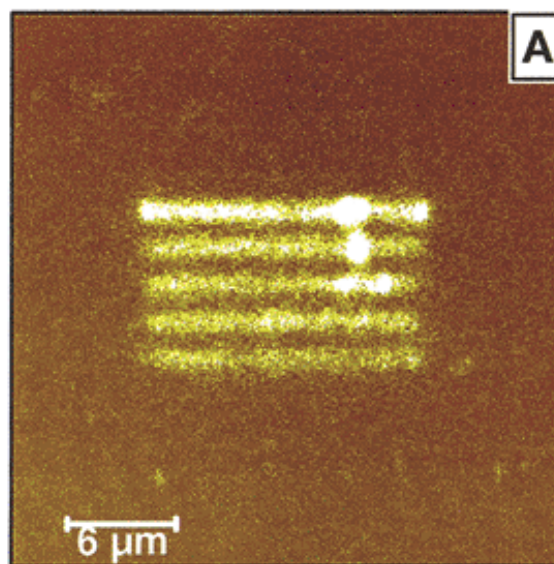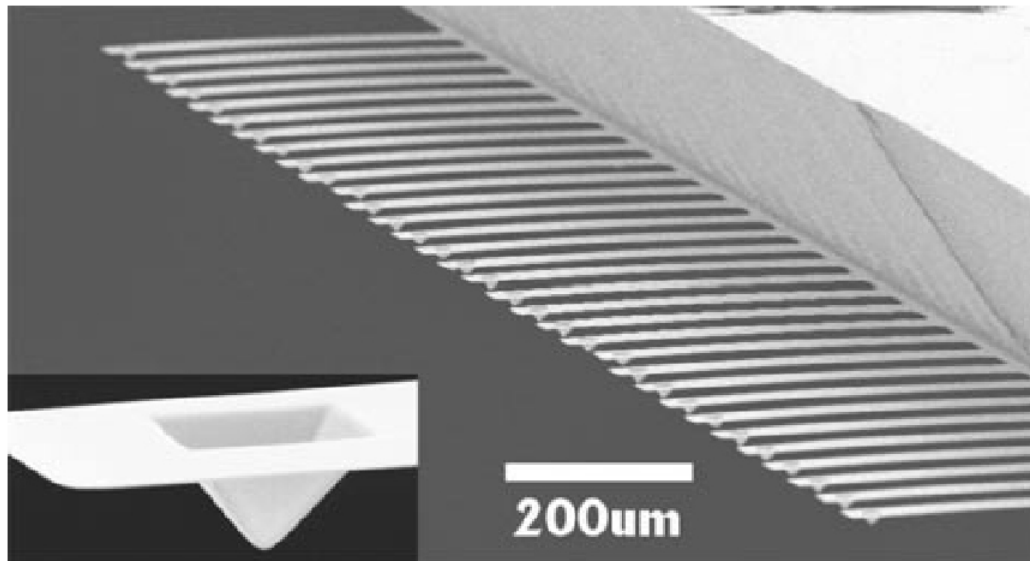
Dip-Pen Nanolithography

TMAFM (Tapping ModeAFM) topographic images of etched MHA(16-mercaptohexadecanoic acid)/Au/Ti/SiO$_x$/Si nanogaps.
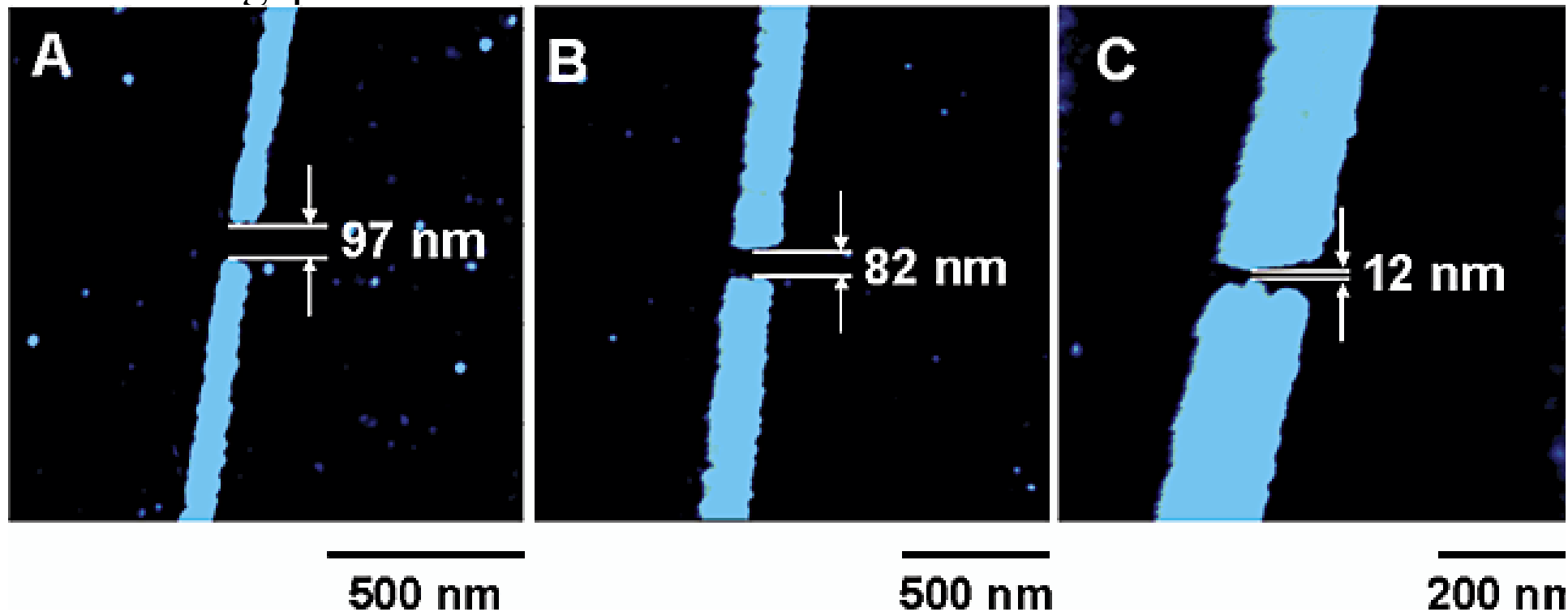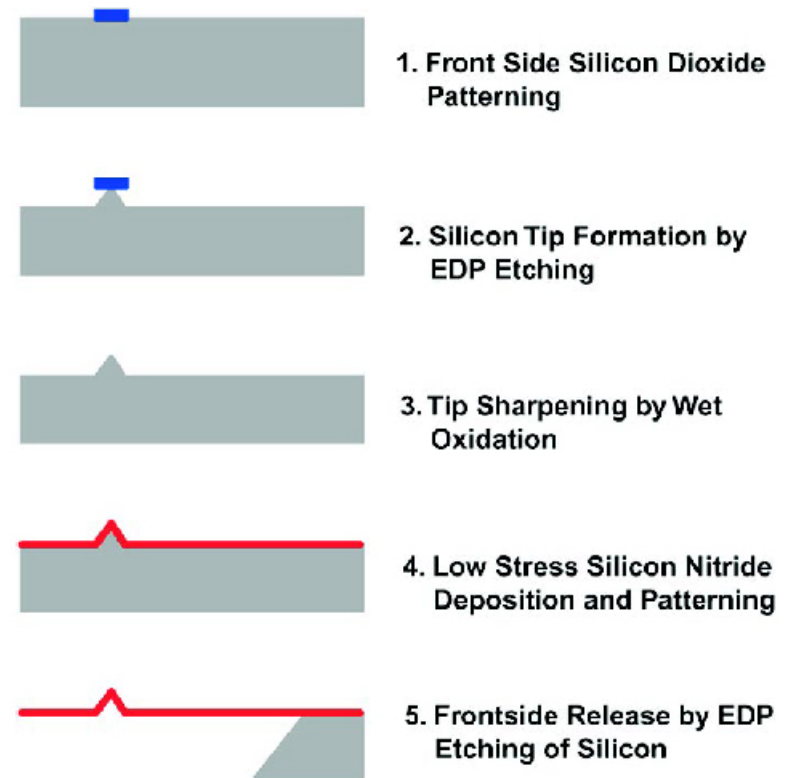
MEMS Nanoplotter

- Microelectromechanical systems micromachining technology

SEM micrograph of a type-1 32 DPN probe array made. The insert shows an enlarged view of a single tip at the end of a beam.
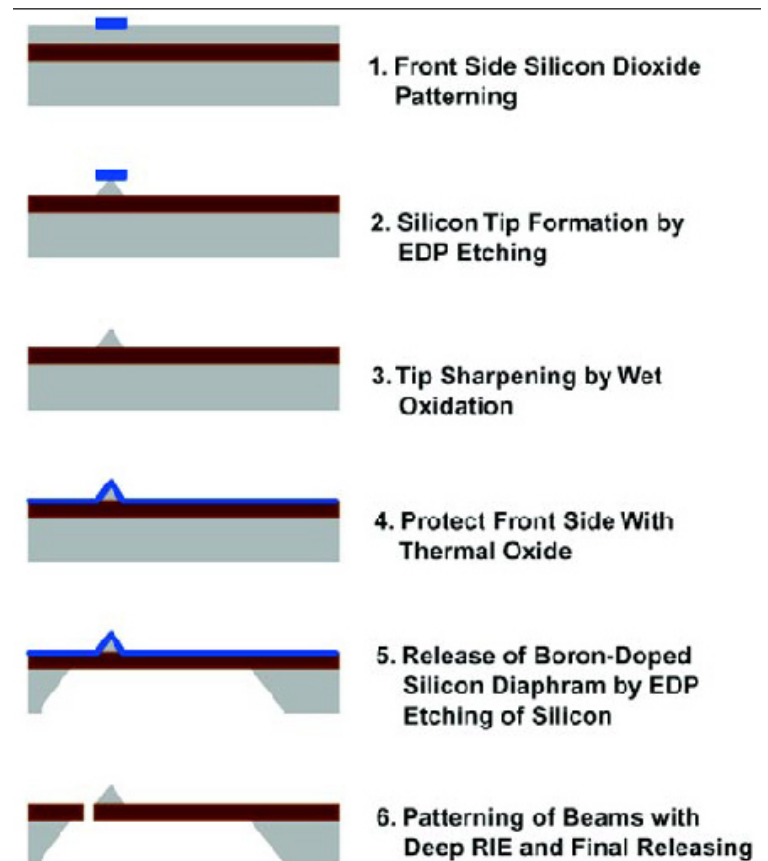

1. Front Side Silicon Dioxide Patterning

2. Silicon Tip Formation by EDP Etching

3. Tip Sharpening by Wet Oxidation

4. Low Stress Silicon Nitride Deposition and Patterning

5. Frontside Release by EDP Etching of Silicon

A schematic diagram of the fabrication process of a type-1 DPN probe array. A {100 }n-type silicon wafer serves as the starting wafer.

MEMS Nanoplotter
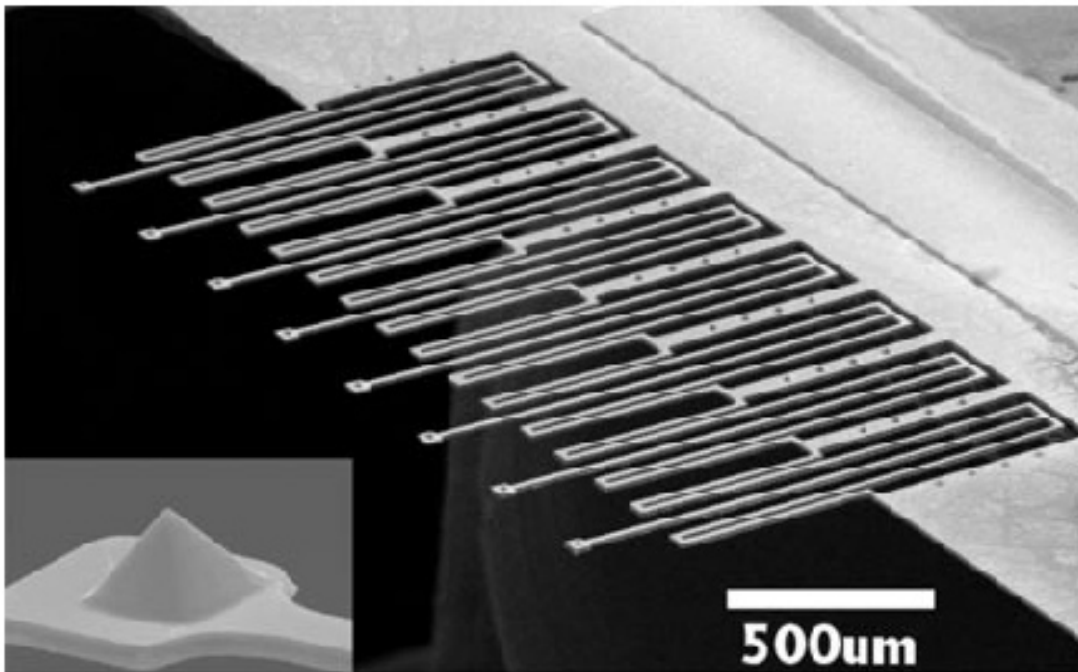
SEM micrograph of a type-2 eight DPN probe array. The insert shows a magnified view of a single tip at the end of a beam. The radius of curvature of this tip is estimated to be 100 nm.

1. Front Side Silicon Dioxide Patterning

2. Silicon Tip Formation by EDP Etching

3. Tip Sharpening by Wet Oxidation

4. Protect Front Side With Thermal Oxide

5. Release of Boron-Doped Silicon Diaphram by EDP Etching of Silicon

6. Patterning of Beams with Deep RIE and Final Releasing

A schematic diagram of the fabrication process of a type-2 DPN probe array. The process initiates from a three-layered silicon wafer that has a heavily boron-doped

MEMS Nanoplotter

LFM images of ODT patterns on a gold surface as written by two adjacent type-1 silicon nitride probes. The writing speed is

0.1 µm s^{-1} . The contact force is estimated as 1.3 nN. The humidity

and the temperature of the ambient are 35% and 23 °C, respectively. The linewidth is 260 nm.

LFM images of ODT patterns on a gold surface as written by two adjacent type-2 silicon probes. The linewidth is 60 nm. The
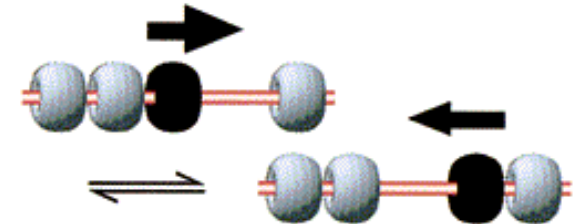
patterns are generated under a
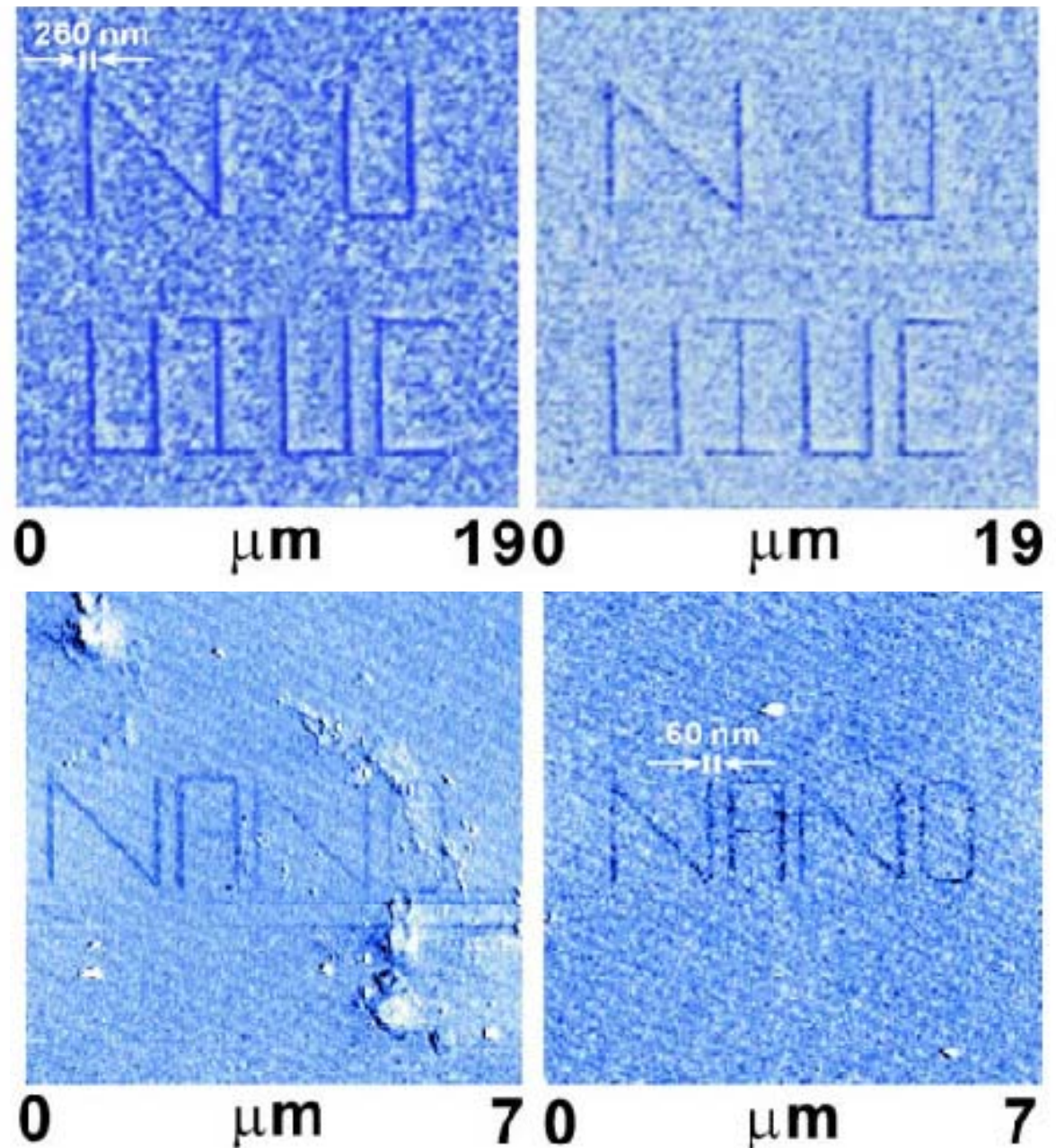
Molecular Abacus

(a) Structure of the "molecular necklace", and
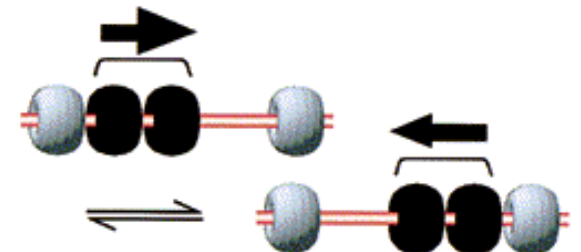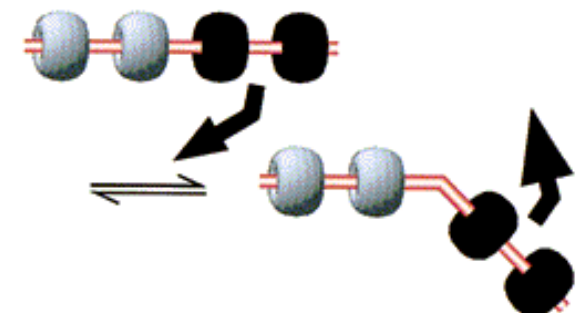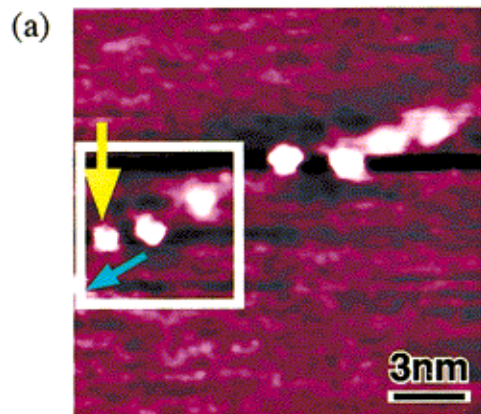three modes (b, c, and d) of the shuttle manipulation by STM.

(a) Molecular Necklace
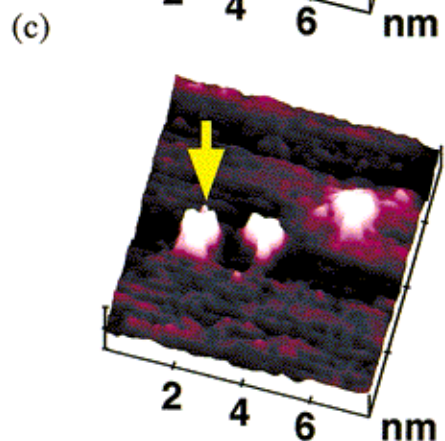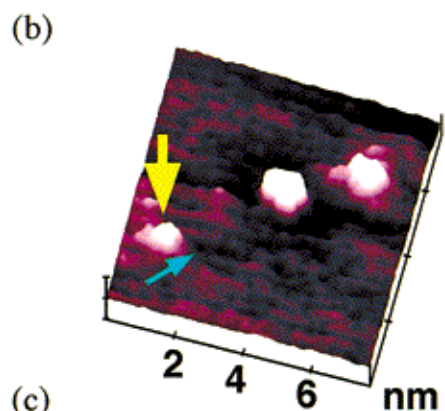
(b) Simple-Shuttling

(c) Pair-Shuttling

(d) Bending

Molecular Abacus

(a)

3nm

(b)

2 4 6 nm

(c)

2 4 6 nm
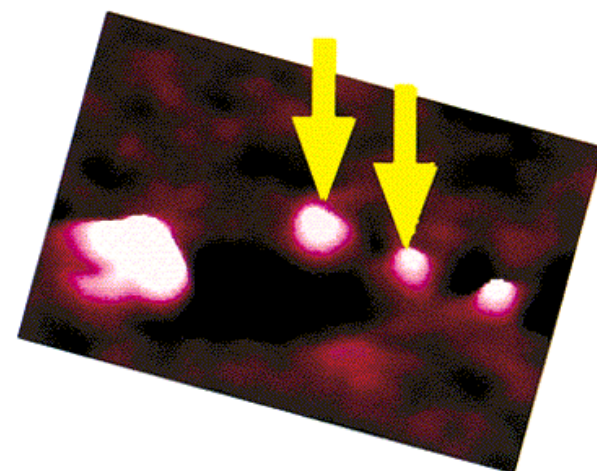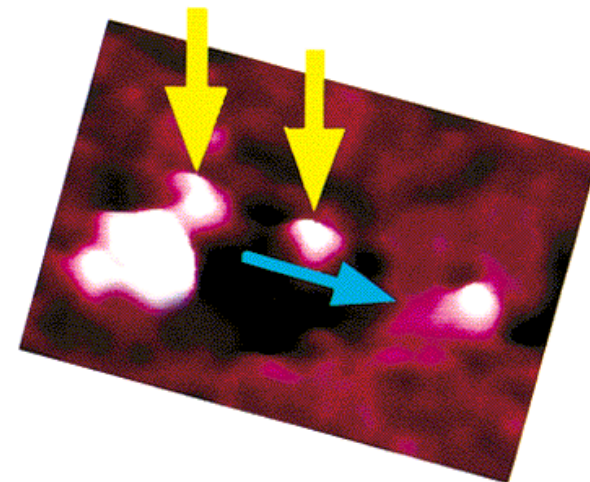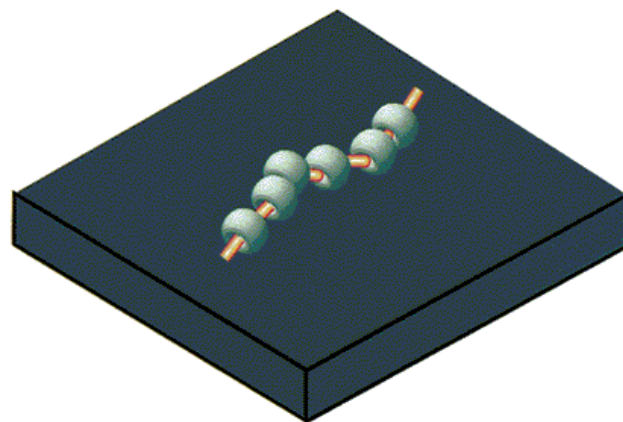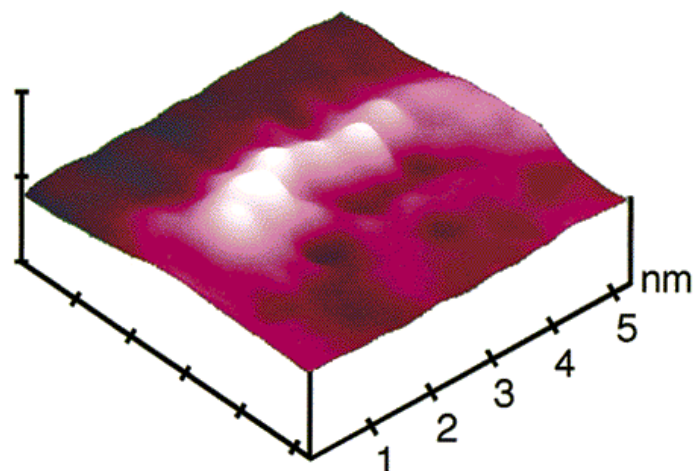
A typical STM image of the molecular necklace (a) and its schematic structure (b).

nm
5
4
3
2
1

STM images of the simple-shuttling (Figure 1b).

STM images of the pair-shuttling (Figure 1c).

Patterning through Polymerisation

Scanning tunnelling microscope (STM) images and diagrams showing the process of controlling the initiation and termination of linear chain polymerization with an STM tip. STM images were obtained in air at room temperature in constant-current mode. *Nature* 2001 **409**, 683
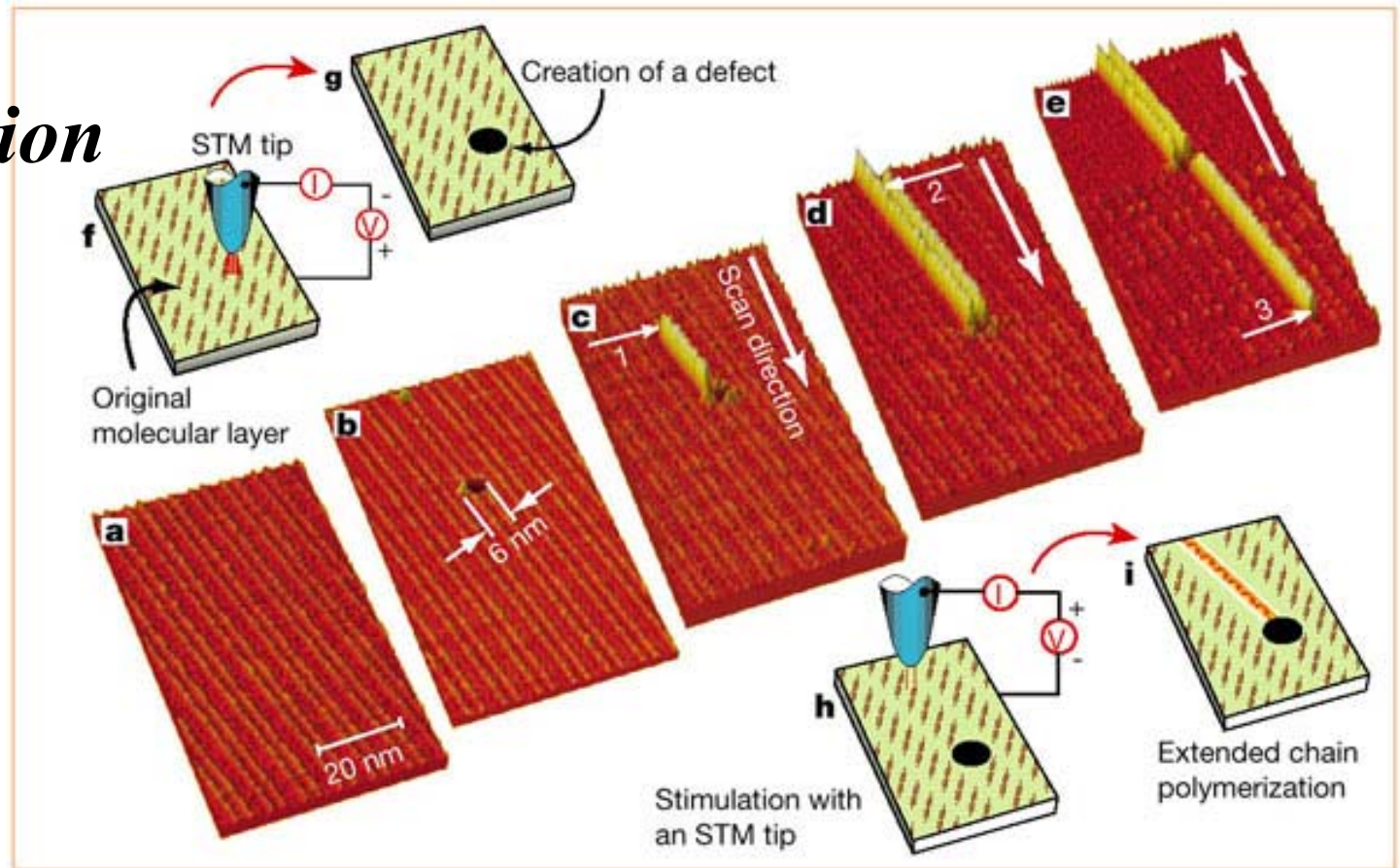

a, STM image of the original monomolecular layer of 10,12-nonacosadiynoic acid.

b, Creation of an artificial defect in advance in the monomolecular layer using an STM tip.

c, First chain polymerization, initiated at the point indicated by arrow (1) using an STM tip, and terminated at the artificial defect.

d, Second chain polymerization, initiated at arrow (2). **e,** Third chain polymerization, initiated at arrow (3).

f, g, Creation of an artificial defect in advance with an STM tip.

h, i, Initiation of chain polymerization with an STM tip, and termination of the polymerization at the artificial defect.

Direct Write - Inkjet

Table I. Ink Composition

Material	Content (vol%)
ZrO_2 powder	14.21
Solsperse 13940	11.85
Isopropyl alcohol	14.21
Octane	56.89
Wax	2.84

Solsperse = aliphatic polyester
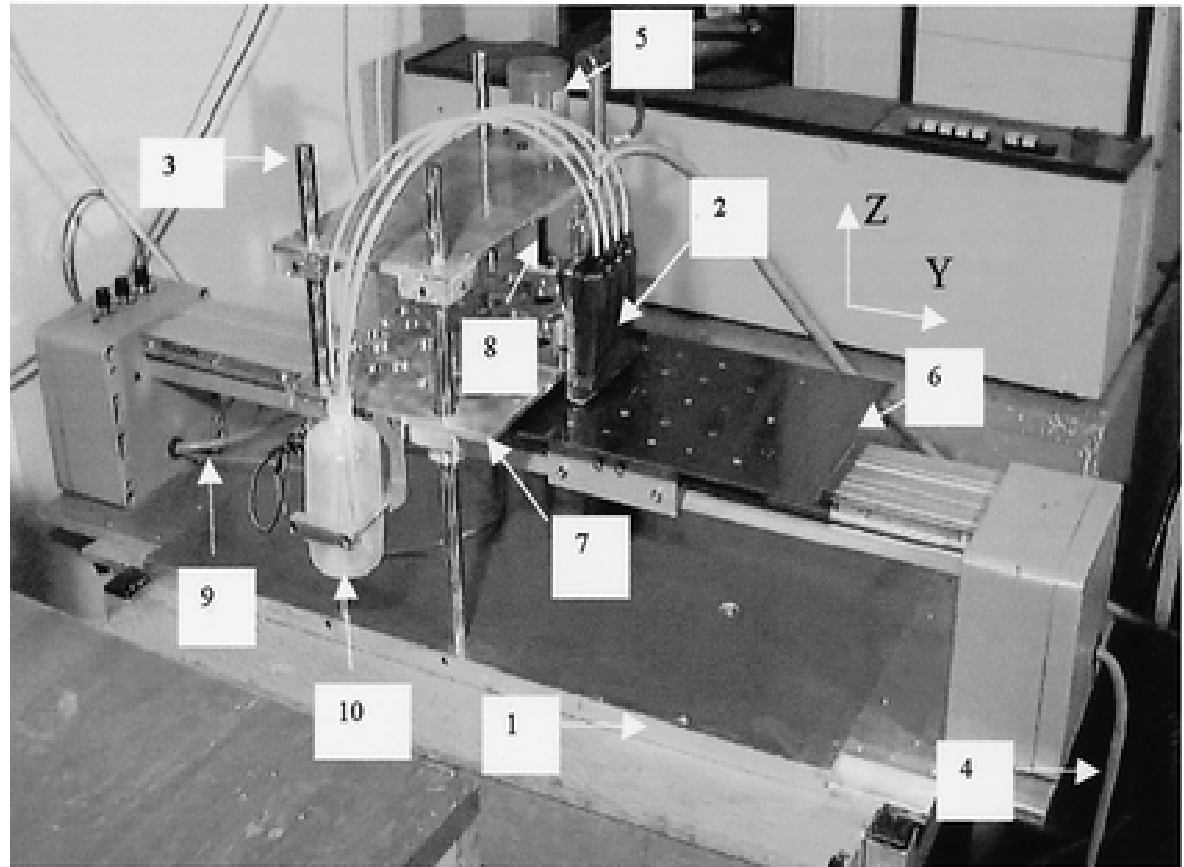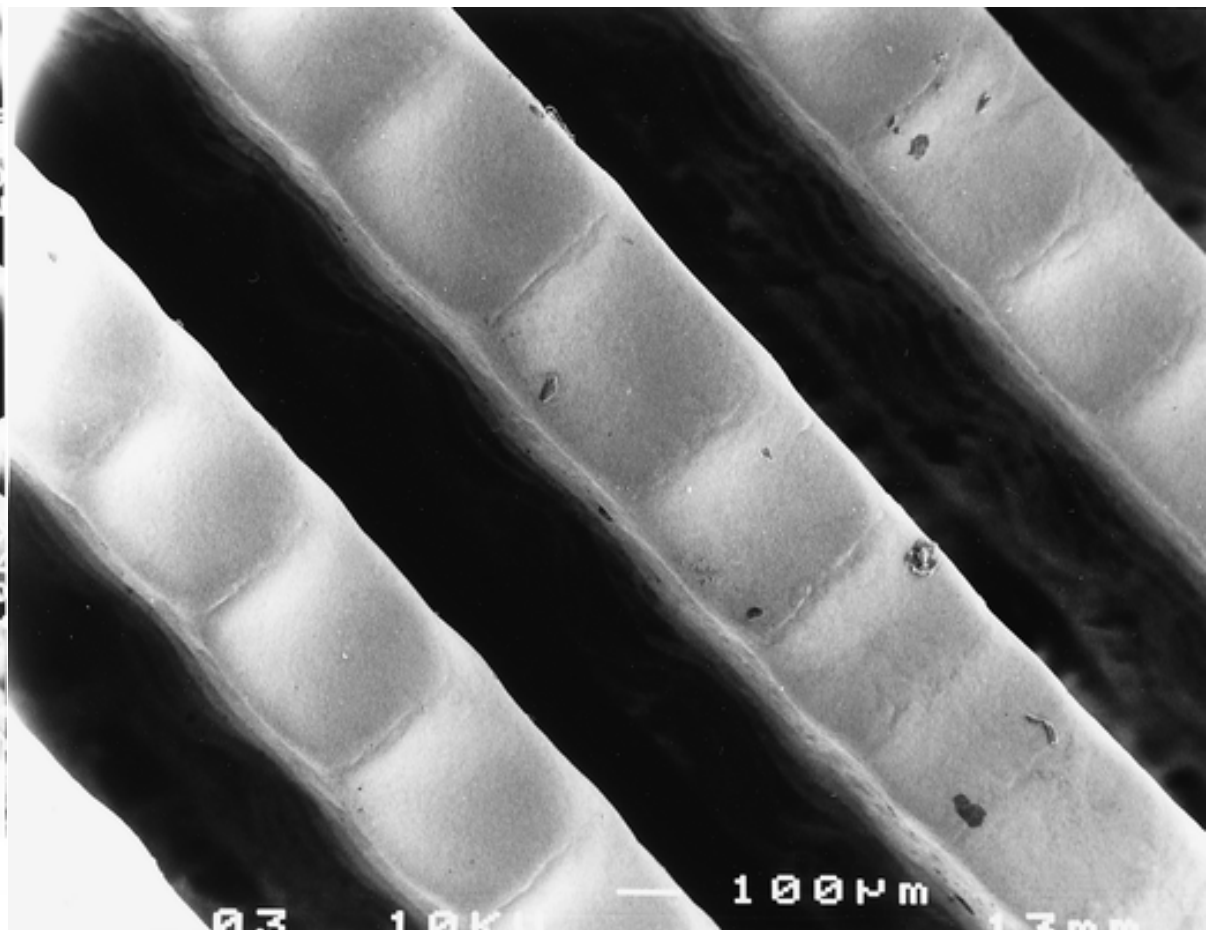

Xaar print-head arranged on a two axis table

1	chassis	2	print head
3	guiding pillar	4	cable to Y-step motor
5	Z-step motor	6	sliding table
7	mounting plate	8	lead screw
9	cable to position sensors	10	ink bottle

Direct Write - Inkjet
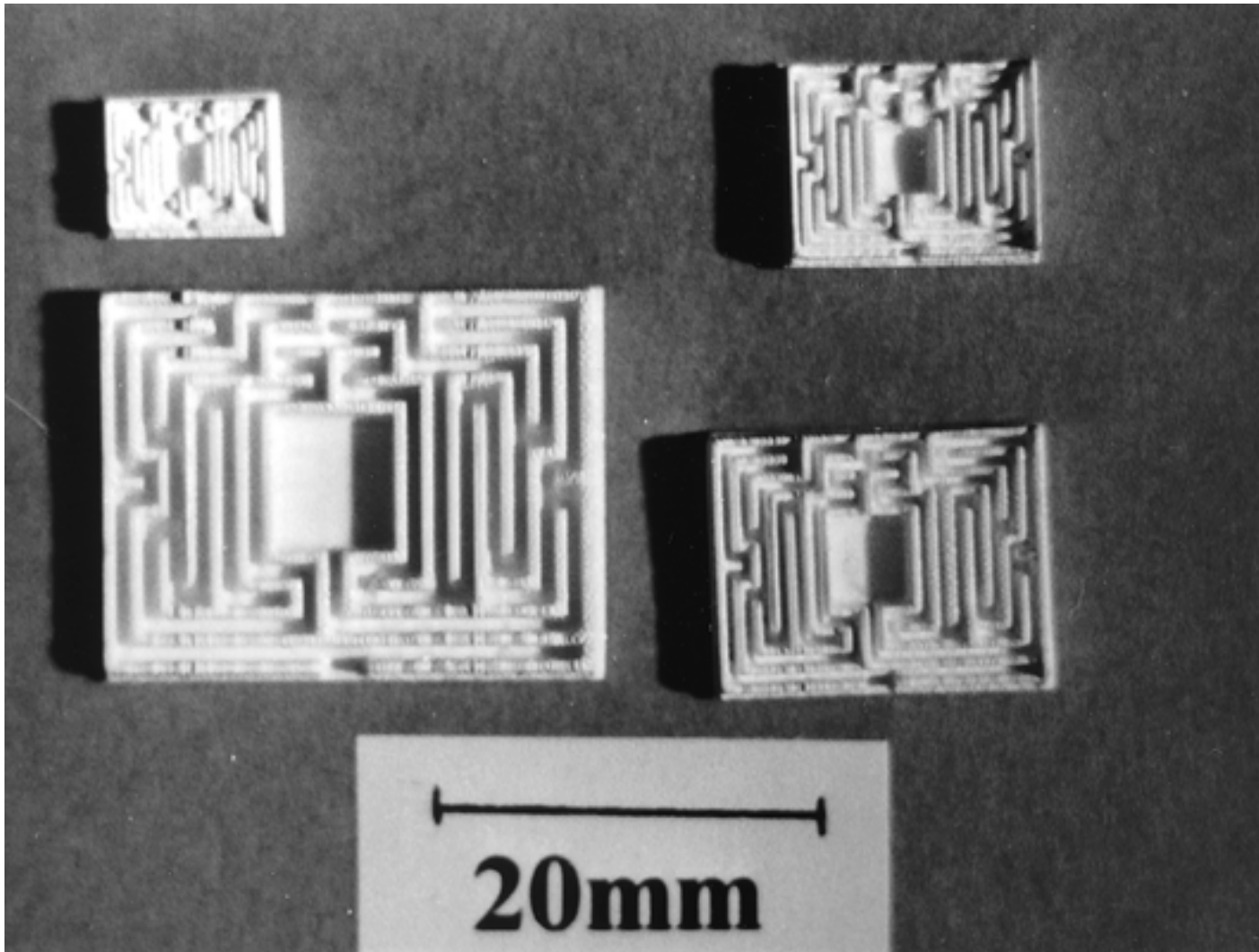
Sintered models of the maze at Hampton Court Palace, U.K.

Direct Write - Inkjet

Top surface of vertical walls of three dots width after sintering.

The End…